
When Rule Violations Are Rare: Chimera Training for Logical Anomaly Detection

1st **Alejandro Ascárate*** 2nd Léo Lebrat* 3rd Rodrigo Santa Cruz*
a.ascaratecastro@hdr.qut.edu.au leo.lebrat@qut.edu.au rodrigo.santacruz@qut.edu.au
4th Clinton Fookes* 5th Olivier Salvado*
c.fookes@qut.edu.au olivier.salvado@qut.edu.au

Abstract

Many practical anomalies are not merely rare inputs, but violations of semantic constraints: objects co-occur in structured ways, actions imply preconditions, and events satisfy temporal or relational regularities. We study anomaly detection in this setting, where constraints are given as logical rules over learned visual concepts, but real rule violations are rare or absent during training. We propose a neural rule evaluator that compiles each constraint into a directed acyclic graph and learns feature-aware subtree MLP gates for its internal logical operators. Each gate maps child features and edge-level negations to a parent representation and a rule-satisfaction probability, with intermediate supervision obtained from exact Boolean propagation over ground-truth concept labels. The key difficulty is that same-image training data often provide insufficient coverage of informative truth configurations and also allow shortcut solutions. To address this, we introduce chimera training: an operand-level counterfactual construction at the feature level. Instead of mixing input images, we concatenate subtree features from different samples; each operand keeps the hard truth label of the sample it came from, and the chimera target is obtained by applying the node’s logical operator to those inherited labels. This supplies supervised logical counterexamples without requiring real anomalous images. Across CLEVRER, OpenImages, and VidOR, the resulting evaluator improves rule-level anomaly AUROC over independent-events and same-image semantic-training baselines, especially for compositional and relational rules. The method yields both scalar anomaly scores and rule-level attributions.

1 Introduction

Detecting anomalies from a dataset is often framed as statistical detection: detecting outliers, samples outside the data distribution (out of distribution, OOD) [Chandola et al., 2009, Hendrycks and Gimpel, 2017, Ruff et al., 2021]. Instead, we are concerned with detecting anomalous samples on the basis of those samples breaking known rules usually satisfied by the initial distribution. This Logical Anomaly Detection approach usually requires to detect and/or learn all the possible logical cases. Our new approach in this paper, describes a method that does not require identifying all the logical cases and can thus detect if a rule is broken when the training dataset contains only samples that are consistent with the rule (missing the anomalous cases). This is a key distinguishing aspect of the anomaly detection problem. In comparison, a fully supervised binary classification would require access to training samples of anomalies, which are by definition rare and usually not accessible in large quantities for training.

*School of Electrical Engineering and Robotics, Faculty of Engineering,
– Queensland University of Technology, Brisbane, Queensland, Australia

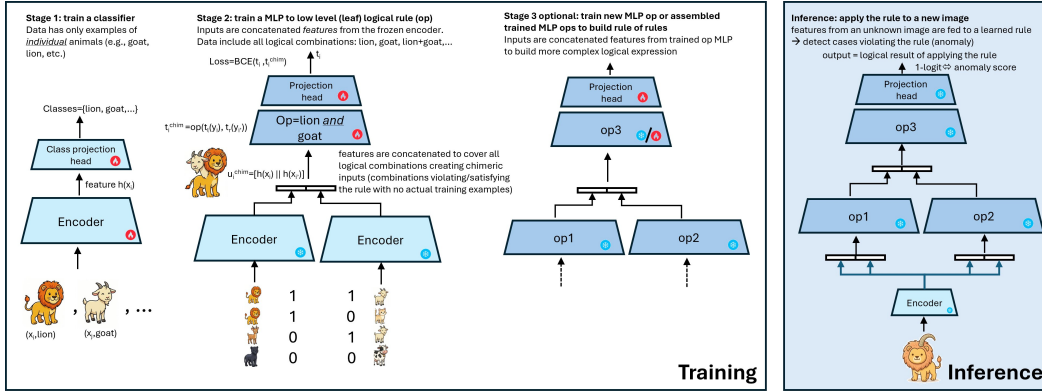


Figure 1: Training and inference of our proposed method. In the first stage a classifier is trained. The head is discarded while the features of the backbone are used next. Each node logical rule needs to be learned using a specific model (stage 2). The backbones of the node rules can be used to learn more complex expressions (stage 3). Once a logical expression has been learned (e.g. a logical ‘and’), it can be frozen and assembled to form more complex rules (alternate stage 3). During inference (stage 4) the frozen ops and classifier backbone are applied to a new image to apply a rule. The output can then be used for anomaly detection or logical inference from the image attributes.

Using the classic simple example of digits classification in MNIST, our method allows detecting all the labeled “7” that look like “1” (see Fig.2). When applied to natural images, one could identify all the atypical presentations in images labeled “(wo)man” as shown in Fig.3 (from the OpenImages dataset). More complex ‘rules’ can be learned as long as they can be expressed as functions of attributes that can be estimated using an appropriate model. We show examples of *causal* rules from videos of basic moving shapes such as “collide(shape=sphere, color=red) \implies collide_before_half_of_video” (using the CLEVRER dataset), and realistic rules on complex and changing scenes in videos such as “obj:baby \implies (rel:baby-in_front_of-adult \wedge rel:adult-watch-baby)” (using the VidOR dataset).

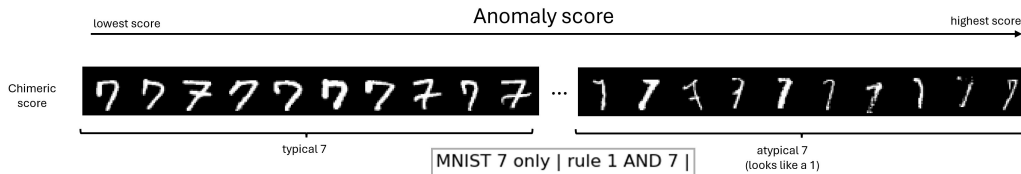


Figure 2: Score-sorted MNIST test images for the rule $1 \wedge 7$, restricted to true digit-7 samples. Images are ordered by increasing learned conjunction score $\hat{P}(1 \wedge 7)$; high-scoring examples correspond to atypical 7’s whose stroke geometry also activates evidence for digit 1.

Thus, many anomaly scenarios are better characterized not merely by “rarity” in pixel (or even latent) space, but by violations of *domain constraints*: objects co-occur in structured ways; actions imply preconditions; and relationships satisfy logical regularities. If such constraints are available (hand-written, mined, or curated), they can serve as a semantically meaningful interface for detection: an input is anomalous if it contradicts one or more constraints.

However, integrating constraint evaluation with high-dimensional perception is nontrivial. Fully symbolic pipelines require brittle perception outputs; fully neural pipelines often re-learn constraints implicitly and entangle them with spurious cues.

This paper proposes a neuro-symbolic anomaly detection framework that treats constraints as *explicit computation graphs* (e.g., *binary trees*) and learns reusable *neural operators* (which we call ‘gates’) that implement logical composition. The method will be referred to as ‘Neural Evaluator’ in the rest of the paper (see Fig.1).

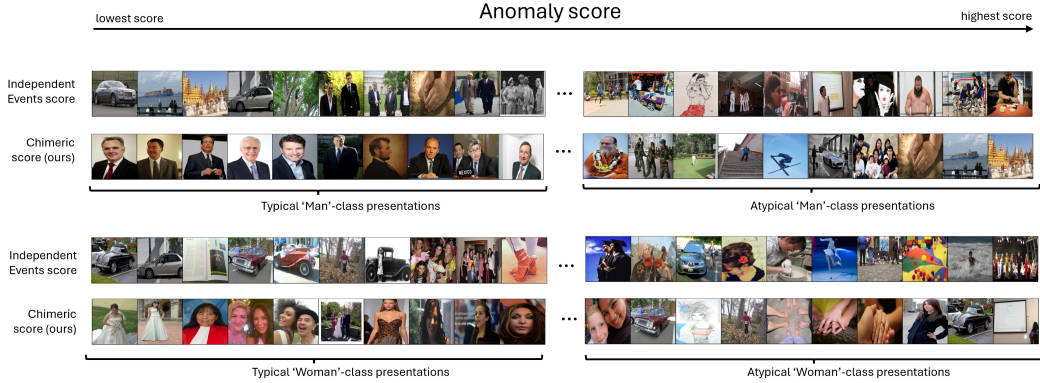


Figure 3: **Qualitative visualization of results for the OpenImages contradiction rule $A \Leftrightarrow \neg A$.** In this experiment, the anomaly score is the model output for the contradiction rule itself (not $1 - p$). Independent Events calculates it only on the basis of the initial classifier’s logits, whereas the chimera training version trains an MLP gate for the rule while additionally introducing synthetic contradictory examples at the feature level that cannot occur in real data. For a fixed test class, we sort samples by anomaly score and show the 10 smallest on the left and the 10 largest on the right. Although all shown images share the same dataset label, the high-score samples are visually more distorted and less prototypical. Chimera produces a visibly cleaner separation, tending to place more normal-looking instances on the left and more abnormal-looking ones on the right, which suggests that the synthetic contradictory supervision helps the evaluator detect within-class visual abnormality more effectively. Upper panel, rule is ‘man $\Leftrightarrow \neg$ man’; lower panel, rule is ‘woman $\Leftrightarrow \neg$ woman’.

A central challenge is preventing gates from collapsing into shortcut classifiers for the entire rule (e.g., recognizing an anomaly template directly from image features). We address this via ‘chimera’² *negative training* (see Fig.1, also Sec.3). This construction is conceptually related to mixup-style interventions [Zhang et al., 2018, Yun et al., 2019], but operates at the level of *subtree operands* rather than raw pixels or labels. Empirically, this encourages gates to behave as compositional operators and improves transfer of learned subtrees across constraints. Furthermore, for many rules, informative counterexamples are exceedingly rare under the natural data distribution (e.g., implication violations require antecedent true and consequent false). Consequently, training a global predictor on real observed samples only yields degenerate solutions (see table 2, ‘SEM’).

Contributions.

- We propose *subtree gates*, a bottom-up node-local-learned evaluator that composes concept-conditioned features into truth probabilities under hard Boolean supervision.
- We introduce *chimera negative training* to enforce operator-level compositionality, reduce shortcut learning in rule evaluators, and to operate in cases where real counterfactuals to the rules are completely absent in the training data (most real applications in anomaly detection).
- We demonstrate effectiveness on structured image/video benchmarks and real-world data (CLEVRER, OpenImages, VidOR).

2 Related Work

Deep anomaly and OOD detection A large body of work scores anomalies using density or reconstruction surrogates (e.g., autoencoders/VAEs), feature-distance criteria, or uncertainty estimates [Chandola et al., 2009, Ruff et al., 2021]. In modern deep OOD detection, common baselines include softmax confidence [Hendrycks and Gimpel, 2017], input perturbation and temperature scaling [Liang et al., 2018, Guo et al., 2017], and feature-space detectors such as Mahalanobis distances [Lee et al., 2018]. Energy-based scoring has also emerged as a unifying view for some classification models

²Wikipedia-Chimera_(mythology).

[Liu et al., 2020]. These approaches typically provide a scalar score with limited semantic attribution: they rarely explain *which* structured expectation is violated.

Semantic and constraint-aware anomaly detection A complementary line leverages structure, constraints, or knowledge to detect implausible samples. Constraint-based and logic-guided learning often imposes penalties for rule violations or encourages outputs to satisfy known relations [Hu et al., 2016, Xu et al., 2018]. Related ideas appear in weakly-supervised and knowledge-driven settings, where symbolic constraints regularize predictors without requiring full labels [Ganchev et al., 2010]. While effective, many methods treat constraints as a global regularizer and do not explicitly construct reusable *modules* implementing logical composition that can be transferred across many rules.

Neuro-symbolic reasoning and differentiable logic Neuro-symbolic methods aim to combine sub-symbolic perception with symbolic reasoning, including differentiable logical frameworks and probabilistic logic programming [d’Avila Garcez et al., 2009, Manhaeve et al., 2018, Donadello et al., 2017]. In vision-and-language and synthetic reasoning benchmarks (e.g., CLEVR), neural module networks and related compositional models assemble learned operators according to an explicit program or graph structure [Andreas et al., 2016, Johnson et al., 2017a]. These works motivate our design choice of compiling constraints into explicit computation graphs. However, much of this literature targets question answering or program execution rather than anomaly detection; and many methods learn operators end-to-end without a mechanism to (i) supervise intermediate truth semantics from ground-truth concepts, (ii) prevent shortcut learning at internal nodes, (iii) deal with highly unbalanced training data for a standard supervised fit, and, (iv) reuse learned subtrees safely across rule sets and runs.

Concept bottlenecks and interpretable interfaces Concept bottleneck models (CBMs) and related “predict-then-reason” pipelines provide an interpretable intermediate representation through human-aligned concepts [Koh et al., 2020]. Our leaf concept bank is similar in spirit: it exposes a semantically meaningful interface for downstream reasoning. Unlike standard CBM pipelines that apply a fixed symbolic reasoner (or a shallow classifier) atop concept predictions, we learn a *structured evaluator* that maps concept-conditioned features through a constraint DAG, producing per-rule satisfaction probabilities and anomaly attributions.

Compositional regularization and counterfactual mixing Data mixing strategies such as mixup and CutMix improve robustness by constructing interpolated or patched examples [Zhang et al., 2018, Yun et al., 2019]. Our *chimera negative training* is related in the sense of creating counterfactual combinations, but differs in locus and supervision: we mix *subtree operands* (child features) rather than raw inputs, and supervise targets using exact Boolean semantics computed from the corresponding hard child truths. This pushes internal gates to implement the intended connective rather than overfitting to global visual templates of a particular rule.

Neural Algebra of Classifiers (NAC) and similar methods, and relation to our evaluator. Neural Algebra of Classifiers (NAC; Santa Cruz et al. [2018]) (other similar methods are [Misra et al., 2017, Nagarajan and Grauman, 2018, Yang et al., 2020, Li et al., 2021]) is the closest conceptual precedent to our work in that it learns neural modules intended to implement Boolean connectives and composes them along an expression tree. However, NAC composes classifier parameters (e.g., weight vectors for primitive concept classifiers) to synthesize a new classifier for a composed expression, and is trained primarily with expression-level supervision (labels for the whole composed concept).

3 Method

3.1 Problem set up, training, and inference

Problem set up We consider a multi-label dataset

$$\mathcal{D} = \{(x_i, y_i)\}_{i=1}^M, \quad y_i \in \{0, 1\}^N, \tag{1}$$

where $y_{i,c} = 1$ indicates that concept c is present in x_i . We are given rules $\{\mathcal{R}_r\}_{r=1}^R$, each compiled into a directed acyclic graph $G_r = (V_r, E_r)$ whose leaves are concept IDs and whose internal nodes are logical operators in {IFF, IMPLIES, AND, OR}. Edges may carry negation flags. The task is to output an anomaly score $s(x) \in [0, 1]$ together with per-rule violation scores $\{s_r(x)\}$.

Training A leaf concept bank first produces

$$z = E_\phi(x) \in \mathbb{R}^F, \quad \ell(x) \in \mathbb{R}^N, \quad p(x) = \sigma(\ell(x)) \in (0, 1)^N. \quad (2)$$

The encoder feature z is used as the evidence carrier for neural rule evaluation, while $p(x)$ is used for scoring.

Each rule graph stores node attributes identifying leaves, concept IDs, and operator codes, and edge attributes encoding negation and, for implications, operand order. Given hard concept labels y , exact Boolean semantics are propagated bottom-up through the graph to obtain node-level targets $t_v(y) \in \{0, 1\}$ for every internal node, not only the root.

For each internal node v with children c_1, \dots, c_{a_v} , we assign a learned subtree gate g_{θ_v} . With child features $h_{c_j} \in \mathbb{R}^F$ and negation indicators $b_j \in \{0, 1\}$, define

$$u_v = [h_{c_1} \| b_1 \| \dots \| h_{c_{a_v}} \| b_{a_v}], \quad (3)$$

$$h_v = f_{\theta_v}(u_v), \quad (4)$$

$$\hat{t}_v = \sigma(w_v^\top h_v + \beta_v). \quad (5)$$

Leaves are initialized with $h_v \leftarrow z = E_\phi(x)$. Thus, rule structure determines which concept role each copy of z plays, while gates learn concept- and operator-specific composition in feature space.

Training is performed bottom-up by depth. For depth level $\mathcal{V}_d = \{v : \text{depth}(v) = d\}$, lower-depth gates are frozen and used to produce child features. Each gate at level d is then trained with node-wise binary cross-entropy,

$$\mathcal{L}_v = \frac{1}{B} \sum_{i=1}^B \text{BCE}(\hat{t}_v(x_i), t_v(y_i)). \quad (6)$$

This internal supervision forces local logical composition rather than a monolithic root-level rule classifier.

To prevent shortcut learning, we use chimera training. For a binary node v with children (ℓ, r) , choose a permutation π with $\pi(i) \neq i$ and form mixed operands

$$(u_v^{\text{chim}})_i = [h_\ell(x_i) \| b_\ell \| h_r(x_{\pi(i)}) \| b_r]. \quad (7)$$

The target is computed by the intended Boolean operator:

$$(t_v^{\text{chim}})_i = \text{op}(v)(t_\ell(y_i), t_r(y_{\pi(i)})). \quad (8)$$

Thus, counterfactual mixing occurs at the operand level, giving informative truth assignments even when some rule outcomes are rare or absent in the observed data.

Finally, to scale across many rules, trained gates are reused through lineage-aware caching. A subtree key records the symbolic subtree, edge negations, operator order, gate architecture, feature dimension, and a fingerprint of the upstream encoder. Hence a cached gate is reused only when both the logical structure and the feature representation match.

Inference and anomaly scoring For each rule r , we evaluate the root satisfaction probability $\hat{t}_{\text{root}}^{(r)}(x) \in (0, 1)$ by bottom-up propagation through the trained/cached gates on G_r (see Algorithm 4), where again we use `dgl.topological_nodes_generator` to great advantage.

Per-rule violation. We define a basic violation score (see Algorithm 5)

$$v_r(x) = 1 - \hat{t}_{\text{root}}^{(r)}(x). \quad (9)$$

Because the scoring is rule-decomposable, the detector naturally provides semantic attributions: the top- k rules with the largest $s_r(x)$ explain the anomaly.

3.2 Why implications are particularly suited for anomaly detection.

Among Boolean connectives, the implication $A \Rightarrow B$ is especially well-matched to anomaly detection because it's *non-symmetric* and its truth table has a *single* and *non-trivial* falsifying

configuration: it is false only when the antecedent holds but the consequent does not, i.e. ($A = 1, B = 0$). Consequently, each implication directly defines a sharp notion of “violation” (our anomaly signal) that is both sparse and interpretable: an anomaly corresponds precisely to the presence of the contextual precondition A together with the absence of the expected outcome B . Equivalently, the implication acts as a *context-gated* detector: when the antecedent is not present ($A = 0$), the rule is vacuously satisfied and produces no alarm (it ignores the sample outside its intended regime of applicability), whereas when the antecedent is present ($A = 1$), the rule activates and flags an anomaly exactly when the consequent is absent ($B = 0$) in that specific context. This “activate-on-context, trigger-on-violation” behavior is precisely what we want in realistic perceptual settings, where we aim to avoid spurious alarms on irrelevant inputs while reliably detecting context-specific inconsistencies.

4 Experiments

4.1 Datasets and concept vocabularies

We evaluate on three vision benchmarks where (i) a multi-label concept inventory is available (or can be induced), and (ii) logical constraints over these concepts are meaningful.

CLEVR (images). We use CLEVR images and their ground-truth scene annotations Johnson et al. [2017b]. **CLEVRER (videos).** We use CLEVRER and its structured annotations Yi et al. [2020]. **Open Images.** We use Open Images V4 annotations Kuznetsova et al. [2018]. **VidOR.** We evaluate on the VidOR (Video Object Relation) dataset Shang et al. [2019].

4.2 Evaluation tasks and metrics

Consistency anomaly detection. We define a binary anomaly label from ground-truth concepts and rules:

$$y_{\text{anom}}(x) = \mathbb{I}\left[\min_{r \leq R} \text{Truth}_r(x) = 0\right],$$

i.e., an example is anomalous iff it violates *at least one* constraint under hard boolean evaluation. We report AUROC and (when useful) FPR@95TPR for anomaly detection.

Concept prediction quality. We report macro AUROC and macro AUPRC over the K concept heads on the held-out split, since rule performance depends on leaf quality.

4.3 Baselines and Comparisons

We consider as baselines only *rule-aware* detectors (use the same concept vocabulary and rule set as our method), since *perception-only* anomaly detectors ignore rules. Unless otherwise stated, all baselines use the same backbone/encoder as the leaf concept bank for a controlled comparison.

4.3.1 Independent-events probabilistic evaluator (INDEPPROB) (Rule-aware symbolic baseline).

Let A, B denote leaf events (concepts) with predicted probabilities p_A, p_B from the leaf bank. Let φ be a rule formula built from leaves using $\neg, \wedge, \vee, \Rightarrow, \Leftrightarrow$. Assume leaf events are **independent** given x , then one computes a soft satisfaction probability $P(\varphi)$ by recursion using the independent events prescriptions in App. D. For a general formula φ , evaluate bottom-up on the compiled rule DAG using these local identities (and applying edge-level negation by $p \mapsto 1 - p$). The anomaly score is then $s_r(x) = 1 - P(\varphi_r | x)$.

4.3.2 Semantic-loss (SEM) training baseline (semantic consistency from ordinary data).

The core idea of SEM is to train with semantic structure as supervision [Xu et al., 2018], rather than relying only on independent per-concept losses or on explicit real or synthetic anomalies. In our setting, this means encouraging the evaluator to learn rule-consistent compositions from ordinary samples: the model is exposed only to concept tuples that arise naturally in the data, and it must infer semantic compatibility or incompatibility from those same-image assignments. Thus, SEM captures the idea that logical or semantic structure can itself serve as a training signal, without requiring the explicit counterfactual/chimeric constructions that are central to our method.

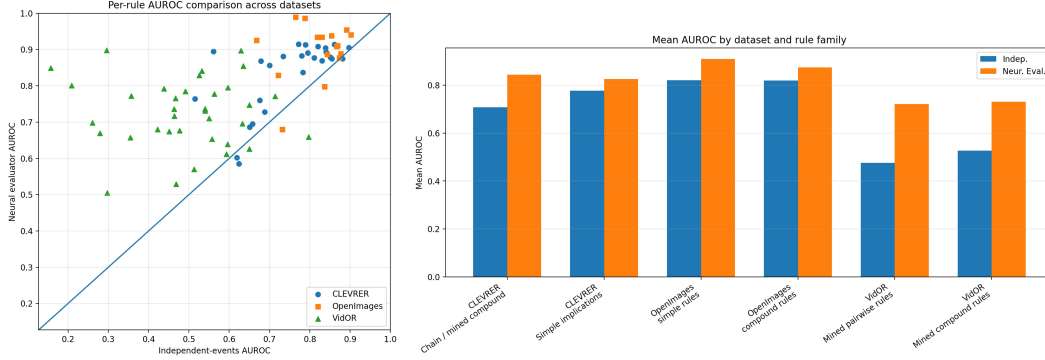


Figure 4: Comparison across datasets (left), and by dataset and rule family (right).

Dataset	Macro ROC-AUC	Macro AP	Macro Acc.
CLEVRER	0.921	0.682	0.867
OpenImages	0.948	0.596	0.904
VidOR	0.679	0.057	0.976

Table 1: Leaf-bank performance on the evaluation split. For VidOR, macro AP is the more informative metric because many relation concepts are extremely sparse, so accuracy is inflated by class imbalance.

Our implementation of SEM. We instantiate SEM in the variant that, in our view, provides the cleanest and fairest comparison with our full model while preserving the core semantic-training idea above. Concretely, SEM uses the same overall compositional evaluator pipeline as our method, but removes chimera-based supervision: all node concepts in a formula are instantiated from features extracted from the same normal image, and no real or synthesized anomalous or counterfactual compositions are introduced during training (since the application here is OOD, real anomalous samples are removed from the training). This keeps the rule compilation, evaluator structure, feature extractor, and test-time scoring protocol aligned with our full system, so that the main difference lies in the training signal itself. Consequently, the gap between SEM and the full model should be interpreted as quantifying the benefit of chimera-based compositional supervision beyond what can be learned from same-image semantic consistency alone.

4.3.3 Monolithic root-only baseline.

To isolate the contribution of our level-wise, node-local modular training scheme, we also consider a monolithic root-only baseline. In this variant, we remove all internal subtree gates and bottom-up supervision, and instead place a single MLP on top of the frozen leaf-bank outputs to predict the root truth value directly for each rule. The baseline therefore retains the same leaf encoder and rule-level target, but discards the explicit decomposition into local operators. We evaluate two versions: one trained only on normal same-image samples, and one additionally trained with chimera-based counterfactual compositions. The latter is the more informative ablation, since it tests whether chimera supervision alone is sufficient, or whether the full benefit of our method also depends on the level-wise and node-local modular structure.

5 Results

Table 1 first shows that the leaf concept bank is already reasonably strong on CLEVRER and OpenImages, whereas VidOR is substantially more challenging, especially for sparse relation concepts. Despite this, the proposed neural evaluator consistently improves rule-level anomaly AUROC over the independent-events baseline (Table 2). On the currently exported rules, the gain is +0.083 on CLEVRER (0.833 vs. 0.750, 23/26 wins), +0.078 on OpenImages (0.899 vs. 0.821, 14/16 wins after excluding one degenerate rule), and +0.234 on VidOR (0.724 vs. 0.490, 33/35 wins). The gains are especially pronounced on compositional rule families, including chain and mined compound rules on

Dataset	Rule family	#Rules	Indep.	SEM	Mono-N	Mono-C	Neur. Eval.	Wins
CLEVRER	Simple implications	16	0.777	0.500	0.500	0.832	0.826	13/16
	Chain & Compound	10	0.707	0.500	0.500	0.827	0.844	10/10
	All rules	26	0.750	0.500	0.500	0.829	0.833	23/26
Std*	-	-	0.011	0.001	0.001	0.010	0.012	-
OpenImages	Simple implications	11	0.821	0.500	0.500	0.906	0.910	10/11
	Compound rules	5	0.820	0.500	0.500	0.880	0.874	4/5
	All rules	16	0.821	0.500	0.500	0.893	0.899	14/16
Std*	-	-	0.013	0.001	0.001	0.012	0.011	-
VidOR	Simple implications	25	0.476	0.500	0.500	0.702	0.722	23/25
	Compound rules	10	0.527	0.500	0.500	0.715	0.731	10/10
	All rules	35	0.490	0.500	0.500	0.708	0.724	33/35
Std*	-	-	0.013	0.001	0.001	0.012	0.013	-

Table 2: Rule-level anomaly AUROC (*in ‘All rules’ on 3 runs). Indep. denotes the independent-events probabilistic evaluator; SEM is the same-image semantic-training ablation; Mono-N and Mono-C denote the monolithic root-only baseline trained, respectively, on normal samples only and with chimera-based counterfactual supervision. “Wins” counts how many rules are improved by the full neural evaluator relative to the independent-events baseline. For OpenImages, one degenerate rule with undefined AUROC was excluded from the aggregate.

Dataset	Rule	Indep.	Neur. Eval.
CLEVRER	Chain: collide(brown, sphere) \rightarrow before_half \rightarrow entered_then_collided	0.561	0.895
CLEVRER	OR type: collide(cube, cyan) \rightarrow (before_half \vee entered_then_collided)	0.679	0.868
OpenImages	Tableware \rightarrow Bottle	0.891	0.954
OpenImages	Land vehicle \rightarrow (Bicycle \wedge Car)	0.765	0.989
VidOR	adult-in_front_of-baby \rightarrow baby-in_front_of-adult	0.467	0.766
VidOR	obj:toy \rightarrow (child-next_to-toy \wedge toy-in_front_of-child)	0.526	0.829

Table 3: Representative rule-level improvements. Full per-rule results are deferred to appendix C.

CLEVRER (+0.137) and both pairwise and compound mined rules on VidOR (+0.246 and +0.204, respectively). This is consistent with our hypothesis that feature-aware local composition captures dependencies that fixed probabilistic evaluation misses.

The SEM ablation collapses in the actual complex anomaly-detection benchmarks (this is quite less trivial than it may look like at first sight, cf. with the simpler MNIST scenario of Fig. 5, where it *does* actually retain some signal, likely thanks to the intrinsic uncertainty from the data). In this variant, we keep the same evaluator pipeline but train only on same-image normal samples and remove all chimera-based counterfactual compositions. Empirically, this drives the model to the trivial all-normal solution: it assigns near-zero anomaly score to essentially every sample, yielding AUROC ≈ 0.5 across rules on the more complex datasets. This is consistent with our motivating hypothesis that, under realistic concept sparsity, ordinary normal data do not provide sufficient coverage of informative violating truth configurations; explicit chimera-based supervision is needed to learn a nontrivial anomaly signal.

Ablation: approximate independence vs. event entanglement. To probe whether the main failure mode of the fixed symbolic baseline is specifically its leaf-event independence assumption, we compare two closely related regimes. In **static CLEVR**, the leaves are mostly unary attribute-existence predicates (e.g., blue_sphere, green_cube, metal_any), for which approximate factorization is often a reasonable first-order model. In **event-rich CLEVRER**, by contrast, we retain the same basic shape/color-style vocabulary but add temporally and relationally structured event predicates such as collide(A,B), collide_before_half(A,B), and entered_then_collided(A,B). These predicates are strongly entangled by construction: collisions couple object pairs, temporal predicates depend on collision times, and several events co-occur non-independently.

This distinction is reflected clearly in the behavior of the independent-events evaluator. On static CLEVR, IndepProb is already essentially perfect on the tested rules (mean AUROC = 0.9995; all rules in the range 0.999–1.000). In contrast, on the currently exported event-rich CLEVRER rules, the same evaluator drops to mean AUROC = 0.750, whereas the learned neural evaluator reaches 0.833

Setup	Rule regime	IndepProb	Neur. Eval.
CLEVR	static attribute rules	0.9995	—
CLEVRER	event-rich rules	0.750	0.833

Table 4: Ablation contrasting a regime where approximate leaf independence is plausible (static CLEVR) with one where collision- and time-derived event predicates induce strong dependence (event-rich CLEVRER). On static CLEVR, the independent-events evaluator is already essentially perfect; on CLEVRER, its performance degrades substantially, while the learned evaluator remains stronger.

on the same rule set. Thus, the degradation is not evidence that explicit symbolic structure is itself inadequate; rather, it strongly supports the view that the main weakness of the fixed symbolic baseline is *misspecification of leaf-event independence*. Once collision-driven event structure is introduced, the factorized evaluator becomes structurally mismatched to the data, while the feature-aware local evaluator remains effective.

Ablation of chimera training. The SEM baseline is not only a baseline against competing approaches, but also an internal ablation of our own training scheme. In this variant, we keep the same overall compositional evaluator pipeline, but remove chimera-based supervision: all node concepts are instantiated using features drawn from the same image, and training uses only normal images, without the synthesized anomalous/counterfactual compositions introduced by chimera sampling. Thus, the comparison between the full model and SEM isolates the contribution of chimera training in a broad sense. The resulting performance gap indicates that the gain of the full method does not come merely from the architecture itself, but from the additional compositional supervision provided by chimera examples, which teaches the evaluator to detect semantically inconsistent concept combinations that are rarely or never observed in same-image normal training data alone.

Ablation of node-local, level-wise training. The chimera-trained monolithic baseline performs similarly to the full neural evaluator. This suggests that, in the present regime, the dominant source of improvement is the chimera-based counterfactual supervision rather than the level-wise modular training scheme itself. In other words, once the model is exposed to informative synthetic rule violations, even a single root-level predictor can recover most of the anomaly signal. The result does not make the modular formulation unimportant—it still provides a more interpretable and reusable decomposition of rule evaluation, *crucially without significant performance loss w.r.t. the monolithic case*—but it indicates that the principal performance bottleneck here was the lack of informative violating configurations in the training data.

6 Discussion and Conclusion

We presented a method to learn and apply logical rules based on attributes that can be learned from the data. The key novelty is that complex rules can be learned without requiring all the logical combinations of attributes to be present in the data. We showed practical applications for anomaly detection in images and complex causality-constrained ones from video.

The approach relies on two assumptions that may be violated in some regimes:

- **Concept interface adequacy.** If the concept vocabulary is too weak (missing predicates needed to express true constraints), then rules become either vacuous or systematically violated, and anomaly detection degenerates.
- **Rule quality.** Mined rules can encode spurious correlations, especially in biased datasets. This can inflate anomaly scores for legitimate but underrepresented cases. Antecedent gating helps for implications, but it is not a complete fix for rule bias.

Our central premise is that many practical “anomalies” are not merely rare inputs, but *constraint violations*. By compiling constraints into explicit DAGs and producing per-rule satisfaction probabilities via our chimera-trained evaluator, the detector returns not only a scalar score but also a structured explanation: which rules (and even which internal subclauses) are most violated. This is qualitatively

different from perception-only OOD scores that are often hard to interpret, and it is difficult to obtain with monolithic end-to-end models without imposing explicit structure.

References

- Varun Chandola, Arindam Banerjee, and Vipin Kumar. Anomaly detection: A survey. *ACM Computing Surveys*, 41(3):1–58, 2009.
- Dan Hendrycks and Kevin Gimpel. A baseline for detecting misclassified and out-of-distribution examples in neural networks. In *International Conference on Learning Representations (ICLR)*, 2017.
- Lukas Ruff, Jacob R. Kauffmann, Robert A. Vandermeulen, Grégoire Montavon, Wojciech Samek, Marius Kloft, Thomas G. Dietterich, and Klaus-Robert Müller. A unifying review of deep and shallow anomaly detection. *Proceedings of the IEEE*, 109(5):756–795, 2021.
- Hongyi Zhang, Moustapha Cisse, Yann N. Dauphin, and David Lopez-Paz. mixup: Beyond empirical risk minimization. In *International Conference on Learning Representations (ICLR)*, 2018.
- Sangdoon Yun, Dongyoon Han, Seong Joon Oh, Sanghyuk Chun, Junsuk Choe, and Youngjoon Yoo. Cutmix: Regularization strategy to train strong classifiers with localizable features. In *IEEE/CVF International Conference on Computer Vision (ICCV)*, 2019.
- Shiyu Liang, Yixuan Li, and R. Srikant. Enhancing the reliability of out-of-distribution image detection in neural networks. In *International Conference on Learning Representations (ICLR)*, 2018.
- Chuan Guo, Geoff Pleiss, Yu Sun, and Kilian Q. Weinberger. On calibration of modern neural networks. In *International Conference on Machine Learning (ICML)*, 2017.
- Kimin Lee, Kibok Lee, Honglak Lee, and Jinwoo Shin. A simple unified framework for detecting out-of-distribution samples and adversarial attacks. In *Advances in Neural Information Processing Systems (NeurIPS)*, 2018.
- Weitang Liu, Xiaoyun Wang, John D. Owens, and Yixuan Li. Energy-based out-of-distribution detection. In *Advances in Neural Information Processing Systems (NeurIPS)*, 2020.
- Zhiting Hu, Xuezhe Ma, Zhengzhong Liu, Eduard Hovy, and Eric P. Xing. Harnessing deep neural networks with logic rules. In *Annual Meeting of the Association for Computational Linguistics (ACL)*, 2016.
- Jingyi Xu, Zilu Zhang, Tal Friedman, Yitao Liang, and Guy Van den Broeck. A semantic loss function for deep learning with symbolic knowledge. In Jennifer Dy and Andreas Krause, editors, *Proceedings of the 35th International Conference on Machine Learning*, volume 80 of *Proceedings of Machine Learning Research*, pages 5502–5511. PMLR, 10–15 Jul 2018. URL <https://proceedings.mlr.press/v80/xu18h.html>.
- Kuzman Ganchev, João Graça, Jennifer Gillenwater, and Ben Taskar. Posterior regularization for structured latent variable models. *Journal of Machine Learning Research*, 11(67):2001–2049, 2010. URL <http://jmlr.org/papers/v11/ganchev10a.html>.
- Artur S. d’Avila Garcez, Luis C. Lamb, and Dov M. Gabbay. *Neural-Symbolic Cognitive Reasoning*. Springer, 2009.
- Robin Manhaeve, Sebastijan Dumančić, Angelika Kimmig, Thomas Demeester, and Luc De Raedt. Deepproblog: Neural probabilistic logic programming. In *Advances in Neural Information Processing Systems (NeurIPS)*, 2018.
- Ivan Donadello, Luciano Serafini, and Artur S. d’Avila Garcez. Logic tensor networks for semantic image interpretation. In *International Joint Conference on Artificial Intelligence (IJCAI)*, 2017.
- Jacob Andreas, Marcus Rohrbach, Trevor Darrell, and Dan Klein. Neural module networks. In *IEEE Conference on Computer Vision and Pattern Recognition (CVPR)*, 2016.

- Justin Johnson, Bharath Hariharan, Laurens van der Maaten, Li Fei-Fei, C. Lawrence Zitnick, and Ross Girshick. Inferring and executing programs for visual reasoning. In *IEEE International Conference on Computer Vision (ICCV)*, 2017a.
- Pang Wei Koh, Thao Nguyen, Yew Siang Tang, Stephen Mussmann, Emma Pierson, Been Kim, and Percy Liang. Concept bottleneck models. In *International Conference on Machine Learning (ICML)*, 2020.
- Rodrigo Santa Cruz, Basura Fernando, Anoop Cherian, and Stephen Gould. Neural algebra of classifiers. In *2018 IEEE Winter Conference on Applications of Computer Vision (WACV)*, pages 729–737. IEEE, 2018. ISBN 978-1-5386-4886-5. doi: 10.1109/WACV.2018.00085.
- Ishan Misra, Abhinav Gupta, and Martial Hebert. From red wine to red tomato: Composition with context. In *Proceedings of the IEEE Conference on Computer Vision and Pattern Recognition (CVPR)*, pages 1792–1801, July 2017.
- Tushar Nagarajan and Kristen Grauman. Attributes as operators: Factorizing unseen attribute-object compositions. In *Proceedings of the European Conference on Computer Vision (ECCV)*, pages 169–185, September 2018.
- Muli Yang, Cheng Deng, Junchi Yan, Xianglong Liu, and Dacheng Tao. Learning unseen concepts via hierarchical decomposition and composition. In *IEEE/CVF Conference on Computer Vision and Pattern Recognition (CVPR)*, June 2020.
- Zeqian Li, Michael Mozer, and Jacob Whitehill. Compositional embeddings for multi-label one-shot learning. In *Proceedings of the IEEE/CVF Winter Conference on Applications of Computer Vision (WACV)*, pages 296–304, January 2021.
- Justin Johnson, Bharath Hariharan, Laurens van der Maaten, Li Fei-Fei, C. Lawrence Zitnick, and Ross Girshick. Clevr: A diagnostic dataset for compositional language and elementary visual reasoning. In *Proceedings of the IEEE Conference on Computer Vision and Pattern Recognition (CVPR)*, 2017b.
- Kexin Yi, Chuang Gan, Yunzhu Li, Pushmeet Kohli, Jiajun Wu, Antonio Torralba, and Joshua B. Tenenbaum. Clevrer: Collision events for video representation and reasoning. In *International Conference on Learning Representations (ICLR)*, 2020. arXiv:1910.01442.
- Alina Kuznetsova, Hassan Rom, Neil Alldrin, Jasper Uijlings, Ivan Krasin, Jordi Pont-Tuset, Shahab Kamali, Stefan Popov, Matteo Mallocci, Tom Duerig, and Vittorio Ferrari. The open images dataset v4: Unified image classification, object detection, and visual relationship detection at scale. *arXiv preprint arXiv:1811.00982*, 2018.
- Xindi Shang, Donglin Di, Junbin Xiao, Yu Cao, Xun Yang, and Tat-Seng Chua. Annotating objects and relations in user-generated videos. In *Proceedings of the 2019 on International Conference on Multimedia Retrieval*, pages 279–287. ACM, 2019.

Appendix

A Method (in extended detail) and Algorithms

A.1 Problem setup and notation

We assume a dataset of inputs and *concept* annotations

$$\mathcal{D} = \{(x_i, y_i)\}_{i=1}^M, \quad y_i \in \{0, 1\}^N, \quad (10)$$

where $y_{i,c} = 1$ indicates that concept $c \in \{1, \dots, N\}$ is present in x_i (multi-label). We are also given a set of R rules $\{\mathcal{R}_r\}_{r=1}^R$. Each rule is compiled into a directed acyclic graph (DAG)

$$G_r = (V_r, E_r), \quad (11)$$

whose leaves correspond to concept IDs and whose internal nodes are logical operators (IFF / IMPLIES / AND / OR). Edges may carry a negation flag, implementing literal negation at the child-to-parent interface.

Our goal is anomaly detection with *semantic attribution*: for a test input x , output (i) an anomaly score $s(x) \in [0, 1]$ and (ii) a decomposition into per-rule violation scores $\{s_r(x)\}$ (and optionally per-node scores).

A.2 Leaf concept bank

We first train a leaf concept bank that exposes:

$$z = E_\phi(x) \in \mathbb{R}^F, \quad (12)$$

$$\ell(x) = (\ell_1(x), \dots, \ell_N(x)) \in \mathbb{R}^N, \quad (13)$$

$$p(x) = \sigma(\ell(x)) \in (0, 1)^N, \quad (14)$$

where E_ϕ is a shared encoder and $\ell_c(x)$ is a concept-specific logit head. Optionally, we apply post-hoc temperature scaling on logits (one scalar $T > 0$) before the sigmoid.

In our implementation, the encoder feature z is the basic evidence carrier for downstream rule evaluation. Concept probabilities $p(x)$ are additionally used for *antecedent gating* in implication-style anomaly scoring (§3.1).

A.3 Rule compilation as a DAG

Each rule \mathcal{R}_r is converted to a DAG G_r with:

- node attributes: `mask` $\in \{0, 1\}$ (leaf vs internal), `x` $\in \{0, 1, \dots, N\}$ (concept id for leaves), and `y` $\in \{1, 2, 3, 4\}$ (operator code at internal nodes: IFF, IMPLIES, AND, OR),
- edge attributes: `neg` $\in \{-1, +1\}$ (negation) and (optionally) `pos` $\in \{0, 1\}$ to enforce operand order for IMPLIES.

Commutative operators (IFF/AND/OR) treat children as an unordered multiset (canonicalized by sorting); IMPLIES is ordered (canonicalized by `pos` if present).

Hard semantics (for supervision). Given a concept label vector $y \in \{0, 1\}^N$, we compute node-level ground-truth truth values $t_v(y) \in \{0, 1\}$ by bottom-up propagation on G_r , applying edge negations at the child interface and then applying the exact Boolean operator at the parent. These $t_v(y)$ provide training targets for every internal node, not only the root.

A.4 Subtree gates: learned, feature-aware logical composition

Each internal node v with arity a_v is assigned a lightweight *subtree gate* g_{θ_v} that maps child features and edge-negation flags to: (i) a parent feature $h_v \in \mathbb{R}^F$ and (ii) a satisfaction probability $\hat{t}_v \in (0, 1)$.

Concretely, for children c_1, \dots, c_{a_v} with features $h_{c_j} \in \mathbb{R}^F$ and negation flags $b_j \in \{0, 1\}$,

$$u_v = [h_{c_1} \parallel b_1 \parallel \dots \parallel h_{c_{a_v}} \parallel b_{a_v}] \in \mathbb{R}^{a_v(F+1)}, \quad (15)$$

$$h_v = f_{\theta_v}(u_v) \in \mathbb{R}^F, \quad (16)$$

$$\hat{t}_v = \sigma(w_v^\top h_v + \beta_v) \in (0, 1). \quad (17)$$

Intuitively, g_{θ_v} is a learned operator specialized to the local connective at v , but it operates in a feature space that can represent richer evidence than a scalar leaf probability.

Leaf features. For a given x , we initialize each leaf node v that corresponds to concept $c(v)$ with a feature derived from the leaf-bank encoder:

$$h_v \leftarrow z = E_{\phi}(x). \quad (18)$$

Although this means all leaves share the same base feature vector, the *rule structure and gate identities* specify which leaf positions correspond to which concepts; gates learn to extract concept-relevant evidence from z in a rule-conditional way. (This choice makes the evaluator robust to noisy scalar concept probabilities, while retaining concept semantics through the graph wiring and supervision.)

A.5 Bottom-up, level-wise training with internal-node supervision

Directly training all gates jointly can be unstable because higher nodes depend on learned representations of lower subtrees. We therefore train *bottom-up* by depth.

Let $\text{depth}(v)$ be the longest path length from any leaf to v , and let $\mathcal{V}_d = \{v : \text{depth}(v) = d\}$. We train levels in increasing depth $d = 1, 2, \dots$ (see Algorithm 3):

1. For each mini-batch $\{(x_i, y_i)\}_{i=1}^B$, compute hard truth targets $t_v(y_i)$ for all nodes by exact propagation (Algorithm 2). This is where the choice of representing rules by graphs becomes particularly useful and elegant at the implementation level: we use DGL’s `dgl.topological_nodes_generator` to generate node frontiers using topological traversal (each item is a tensor recording the nodes from bottom level to the roots).
2. Compute leaf encoder features $z_i = E_{\phi}(x_i)$ and initialize leaf node features.
3. Propagate through already-trained lower-depth gates (and keep them fixed) to obtain child features for nodes in \mathcal{V}_d .
4. For each $v \in \mathcal{V}_d$, update gate parameters by minimizing node-wise BCE:

$$\mathcal{L}_v = \frac{1}{B} \sum_{i=1}^B \text{BCE}(\hat{t}_v(x_i), t_v(y_i)). \quad (19)$$

This *internal supervision* is crucial: the model learns to implement logical composition locally, rather than only learning a monolithic “rule classifier” at the root.

A.6 Chimera negative training: enforcing compositionality and preventing shortcut learning

A key failure mode is *shortcut learning*: a gate (or an entire rule) can be predicted directly from global visual features, without respecting the intended operator semantics. We introduce *chimera negatives* to force gates to behave compositionally.

Consider a binary node v with (ordered) children (ℓ, r) and operator $\text{op}(v)$. For a batch of size B , choose a permutation π with $\pi(i) \neq i$ (e.g., a random nontrivial cyclic shift). We form *chimera pairs* by combining the left child from sample i with the right child from a different sample $\pi(i)$:

$$(u_v^{\text{chim}})_i := [h_{\ell}(x_i) \parallel b_{\ell} \parallel h_r(x_{\pi(i)}) \parallel b_r]. \quad (20)$$

Targets are computed *semantically* from the corresponding hard truths (including edge negations):

$$(t_v^{\text{chim}})_i := \text{op}(v)(t_{\ell}(y_i), t_r(y_{\pi(i)})) \in \{0, 1\}. \quad (21)$$

Training batches can include: (i) same-image pairs, optionally restricted to samples where the full rule holds (“AD-strict”), and (ii) chimera pairs (Algorithm 3). This construction breaks correlations that enable shortcut solutions, because the two operands are decoupled across samples while the supervision remains the exact logical composition. In practice, chimera training substantially improves transfer of learned subtrees across rules and reduces overfitting to rule-specific visual templates: only the true relevant features for the rule to hold or not end being recognized.

Novel insight. Chimera training moves counterfactual mixing to the operand level, supplying informative truth assignments even when specific rule outcomes have little or no support in the observed training data.

A.7 Lineage-aware caching: safe reuse of learned subtrees

To scale to many rules, we reuse trained gates across rule graphs whenever the corresponding subtrees match. However, naive caching is unsafe: if the upstream encoder changes, the meaning of features changes. We therefore define a *lineage-aware* cache key $K(v)$ recursively:

$$K(v) = \begin{cases} \text{LEAF}(c(v) \mid \text{enc} = \text{fp}(E_\phi)) & \text{if } v \text{ is a leaf,} \\ \text{OP_OP}(v)(\tilde{K}(c_1), \dots, \tilde{K}(c_{a_v})) \mid \text{arch} \mid F & \text{if } v \text{ is internal,} \end{cases} \quad (22)$$

$$\tilde{K}(c_j) = \begin{cases} K(c_j) & \text{if edge } (c_j \rightarrow v) \text{ is non-negated,} \\ !K(c_j) & \text{if edge } (c_j \rightarrow v) \text{ is negated,} \end{cases} \quad (23)$$

where $\text{fp}(E_\phi)$ is a short fingerprint (hash) of encoder weights, `arch` tags the gate architecture version, and F is the feature dimension. We hash $K(v)$ to obtain a stable filename and store the gate state dict. A cached gate is reused iff the key matches exactly.

A.8 Algorithms

Algorithm 1 $\text{HardOp}(op, \text{vals})$ — exact Boolean semantics used by PROPAGATEHARDTRUTHS

Require: Operator code $op \in \{1, 2, 3, 4\}$ and child truth list $\text{vals}[1..m]$ with $m = |\text{vals}|$.

Ensure: Hard truth $t \in \{0, 1\}$.

```
1: if  $op = 1$  then
2:   (IFF)
3:    $t \leftarrow 1$  (empty list returns 1)
4:   for  $j = 2$  to  $m$  do
5:     if  $\text{vals}[j] \neq \text{vals}[1]$  then
6:        $t \leftarrow 0$ 
7:     end if
8:   end for
9: else
10:  if  $op = 2$  then
11:    (IMPLIES)
12:    if  $m \neq 2$  then
13:       $t \leftarrow 1$ 
14:    else
15:       $a \leftarrow \text{vals}[1]; b \leftarrow \text{vals}[2]$ 
16:       $t \leftarrow (1 - a) \text{ or } b$ 
17:    end if
18:  else
19:    if  $op = 3$  then
20:      (AND)
21:       $t \leftarrow 1$  (empty list returns 1)
22:      for  $j = 1$  to  $m$  do
23:        if  $\text{vals}[j] = 0$  then
24:           $t \leftarrow 0$ 
25:        end if
26:      end for
27:    else
28:      if  $op = 4$  then
29:        (OR)
30:         $t \leftarrow 0$  (empty list returns 0)
31:        for  $j = 1$  to  $m$  do
32:          if  $\text{vals}[j] = 1$  then
33:             $t \leftarrow 1$ 
34:          end if
35:        end for
36:      else
37:         $t \leftarrow 0$ 
38:      end if
39:    end if
40:  end if
41: end if
42: return  $t$ .
```

Algorithm 2 PROPAGATEHARDTRUTHS(G_r, y_i) — hard-truth propagation (core loop)

Require: Rule DAG $G_r = (V, E)$ with node attrs: $\text{mask}[v] \in \{0, 1\}$ (1=leaf), $\mathbf{x}[v] \in \{0, 1, \dots, K\}$ (concept id), $\mathbf{y}[v] \in \{1, 2, 3, 4\}$ (1=IFF, 2=IMPLIES, 3=AND, 4=OR); and edge attr $\text{neg}[e] \in \{-1, +1\}$ (optional).

Require: Concept hard labels $y_i \in \{0, 1\}^K$ indexed by concept id $1..K$.

Ensure: Node hard truth vector $t \in \{0, 1\}^{|V|}$, stored as $G_r.\text{ndata}[\text{'truth_value'}]$.

```
1: Initialize  $t[v] \leftarrow 0$  for all  $v \in V$ .
2: Leaf init by concept id
3: for each node  $v \in V$  do
4:   if  $\text{mask}[v] = 1$  then
5:      $c \leftarrow \mathbf{x}[v]$ 
6:     if  $c > 0$  then
7:        $t[v] \leftarrow y_i[c]$ 
8:     end if
9:   end if
10: end for
11: Bottom-up pass in topological order
12: Let  $\pi$  be a topological ordering of  $V$  where children precede parents.
13: for each node  $v$  in  $\pi$  do
14:   if  $\text{mask}[v] = 0$  then
15:      $(\text{src}, \text{eid}) \leftarrow G_r.\text{in\_edges}(v, \text{form}=\text{'all'})$ .
16:      $m \leftarrow |\text{src}|$ ; create array  $\text{vals}[1..m]$ .
17:     for  $j = 1$  to  $m$  do
18:        $u \leftarrow \text{src}[j]$ ;  $e \leftarrow \text{eid}[j]$ ;  $\text{vals}[j] \leftarrow t[u]$ .
19:       if  $\text{neg}$  exists and  $\text{neg}[e] = -1$  then
20:          $\text{vals}[j] \leftarrow 1 - \text{vals}[j]$ .
21:       end if
22:     end for
23:      $op \leftarrow \mathbf{y}[v]$ .
24:      $t[v] \leftarrow \text{HardOp}(op, \text{vals})$ 
25:   end if
26: end for
27:  $G_r.\text{ndata}[\text{'truth\_value'}] \leftarrow t$ .
28: return  $t$ .
```

(Alg. 1)

Algorithm 3 Training: Leaf Bank + Cached Subtree Gates (Level-wise with Chimera Negatives)

Require: Training set $\mathcal{D}_{\text{train}} = \{(x_i, y_i)\}$ with concept labels $y_i \in \{0, 1\}^K$; rule set $\{\mathcal{R}_r\}_{r=1}^R$ compiled into DAGs $\{G_r\}$; feature dim F ; gate architecture tag arch; negatives mode neg_mode; cache directory \mathcal{C}

Ensure: Leaf concept bank parameters ϕ ; cached gate parameters in \mathcal{C}

- 1: **(A) Train leaf concept bank**
- 2: Initialize encoder+heads ϕ (shared encoder E_ϕ , K sigmoid heads)
- 3: **for** epoch = 1 to E_{leaf} **do**
- 4: **for** mini-batch $\{(x_i, y_i)\}_{i=1}^B$ **do**
- 5: $z_i \leftarrow E_\phi(x_i)$; logits $\ell_i \leftarrow H_\phi(z_i)$
- 6: Update ϕ by minimizing multi-label BCEWithLogits(ℓ_i, y_i) (optionally with pos_weight)
- 7: **end for**
- 8: **end for**
- 9: **if** use_temp_scaling **then**
- 10: Fit scalar temperature T on held-out logits by minimizing BCE($\sigma(\ell/T), y$); store calibrator
- 11: **end if**
- 12: **(B) Train rule evaluators as reusable subtree gates**
- 13: Compute encoder fingerprint fp \leftarrow Fingerprint(E_ϕ)
- 14: **for** each rule graph G_r **do**
- 15: Let $D_{\text{max}} \leftarrow$ maximum internal-node depth in G_r
- 16: **for** depth $d = 1$ to D_{max} **do**
- 17: Let $\mathcal{V}_d \leftarrow \{v \in V_r : \text{depth}(v) = d\}$
- 18: Load or initialize gates $\{g_{\theta_v}\}_{v \in \mathcal{V}_d}$ from cache using lineage key $K(v; \text{fp}, \text{arch}, F)$
- 19: **for** mini-batch $\{(x_i, y_i)\}_{i=1}^B$ **do**
- 20: **Hard node targets:** $t_{v,i} \leftarrow$ PropagateHardTruths(G_r, y_i) $\forall v$
- 21: **Leaf evidence:** $z_i \leftarrow E_\phi(x_i)$; $p_i \leftarrow \sigma(\ell_i)$ from leaf heads
- 22: Initialize leaf node features $h_{\text{leaf}} \leftarrow z_i$ (placed by concept id); leaf probs $\hat{t}_{\text{leaf}} \leftarrow p_i$
- 23: Propagate already-trained lower-depth gates to compute $(h_{c,i}, \hat{t}_{c,i})$ for all children of nodes in \mathcal{V}_d
- 24: **for** each node $v \in \mathcal{V}_d$ **do**
- 25: Build **same-image** inputs $u_{v,i}^{\text{same}} = [h_{c_1,i} \| b_1 \| \dots \| h_{c_a,i} \| b_a]$
- 26: Set targets $t_{v,i}^{\text{same}} = t_{v,i}$
- 27: **if** neg_mode uses chimera **and** v is binary **then**
- 28: Choose a permutation π with $\pi(i) \neq i$
- 29: Build **chimera** inputs $u_{v,i}^{\text{chim}} = [h_{\ell,i} \| b_\ell \| h_{r,\pi(i)} \| b_r]$
- 30: Set targets $t_{v,i}^{\text{chim}} = \text{Op}_v(t_{\ell,i}, t_{r,\pi(i)})$ (with edge negations applied in the hard truths)
- 31: Concatenate training pairs $(u_v, t_v) \leftarrow (u^{\text{same}}, t^{\text{same}}) \cup (u^{\text{chim}}, t^{\text{chim}})$ (optionally filter same-image pairs, e.g. ‘‘AD-strict’’)
- 32: **else**
- 33: $(u_v, t_v) \leftarrow (u^{\text{same}}, t^{\text{same}})$
- 34: **end if**
- 35: Update θ_v by minimizing $\frac{1}{|u_v|} \sum \text{BCE}(g_{\theta_v}(u_v), t_v)$
- 36: **end for**
- 37: **end for**
- 38: Save gates $\{g_{\theta_v}\}$ to cache \mathcal{C} under lineage keys $K(v; \text{fp}, \text{arch}, F)$
- 39: **end for**
- 40: **end for**
- 41: **return** ϕ and cache \mathcal{C}

Algorithm 5 Inference: Rule Satisfaction, Violation Attribution, and Anomaly Scoring

Require: Test input x ; trained leaf bank ϕ (and optional temperature T); rule graphs $\{G_r\}$; gate cache \mathcal{C} ; aggregation mode Agg ; implication gate threshold τ

Ensure: Anomaly score $s(x)$; per-rule scores $\{s_r(x)\}$; top- k violated rules

- 1: Compute encoder feature $z \leftarrow E_\phi(x)$
- 2: Compute concept probabilities $p \leftarrow \sigma(\ell/T)$ (use $T=1$ if no calibration)
- 3: **for** each rule graph G_r **do**
- 4: Load any missing gates from cache \mathcal{C} (by lineage key) into runtime registry
- 5: **Predict root satisfaction:** $p_r(x) \leftarrow \text{PredictRoot}(G_r, z, p; \mathcal{C})$ // bottom-up gate propagation
- 6: **if** G_r is an implication rule with antecedent concept A_r (or antecedent subgraph) **then**
- 7: $a_r \leftarrow p(A_r)$ // antecedent probability from leaf bank
- 8: $g(a_r) \leftarrow \max(0, a_r - \tau)/(1 - \tau)$ // $\tau = 0$ gives identity
- 9: **Antecedent-weighted violation:** $s_r(x) \leftarrow g(a_r) \cdot (1 - p_r(x))$
- 10: **else**
- 11: **Violation:** $s_r(x) \leftarrow 1 - p_r(x)$
- 12: **end if**
- 13: **end for**
- 14: **Aggregate:** $s(x) \leftarrow \text{Agg}(\{s_r(x)\}_{r=1}^R)$ // e.g. max/mean/geo/learned
- 15: **Attribution:** return top- k rules by descending $s_r(x)$ (and optionally the most-violated internal nodes)
- 16: **return** $s(x)$ and $\{s_r(x)\}$

B Datasets and concept vocabularies

We evaluate on three vision benchmarks where (i) a multi-label concept inventory is available (or can be induced), and (ii) logical constraints over these concepts are meaningful.

CLEVR (images). We use CLEVR images and their ground-truth scene annotations Johnson et al. [2017b]. Each concept is a unary predicate of the form “ \exists object with attributes matching a filter”. Concretely, our base concept bank contains $K=6$ attribute filters (e.g., `blue_sphere`, `metal_any`, `gray_cyl`), and an image-level label $y_k \in \{0, 1\}$ is positive iff at least one object in the scene satisfies the corresponding filter.

CLEVRER (videos). We use CLEVRER and its structured annotations Yi et al. [2020]. We reuse the same $K=6$ base attribute-filter concepts for object existence, computed from the per-video object annotations (positive iff the video contains at least one object matching the filter). Optionally (and in the “event-rich” setting), we extend the concept vocabulary with event predicates constructed from CLEVRER event annotations: `enter(A)`, `exit(A)`, `collide(A,B)`, `collide_before_half(A,B)`, and `entered_then_collided(A,B)` where A, B are attribute filters. We cap the number of attribute-pair instantiations (hyperparameter `max_event_pairs`) to keep the rule set tractable.

Open Images. We use Open Images V4 annotations Kuznetsova et al. [2018] and restrict to a manageable concept set by selecting the top- K most frequent detection classes in the validation bounding-box CSV (default $K=50$). A concept label is positive iff an image has *at least one* bounding box of that class. Since Open Images does not provide a canonical train/val split for this exact “consistency anomaly” task, we split the validation images into a *rule/gate-train* partition and an *eval* partition (default `val_train_frac=0.9`).

VidOR. We evaluate on the VidOR (Video Object Relation) dataset Shang et al. [2019], a large-scale collection of 10,000 user-generated videos (98.6 hours) with spatio-temporal annotations of object trajectories and relation instances (80 object categories, 50 relation predicates), using the official split of 7,000/835/2,165 videos for train/val/test. Since test annotations are not fully available, we follow a train \rightarrow val protocol. From training annotations, we construct a multi-label concept vocabulary of K leaves consisting of (i) `obj : c` for the top- K_{obj} most frequent object categories and (ii) `rel : s-p-o` for the top- K_{rel} most frequent relation triplets (subject category s , predicate p , object category o), keeping only triplets with at least a minimum support count. For each video, we uniformly sample T frames and form a multi-hot label vector $y \in \{0, 1\}^K$: an object leaf is positive if its annotated trajectory is present in any sampled frame; a relation leaf is positive if any annotated relation instance is active in at least one sampled frame (with temporal extent $[t_{\text{begin}}, t_{\text{end}}]$). Whenever a relation is labeled positive, we additionally mark its subject and object categories as present, enforcing the structural constraint `rel : s-p-o \Rightarrow (obj : s \wedge obj : o)` at the ground-truth label level. We train a video leaf bank as a multi-label classifier with a shared 2D CNN applied per-frame and mean temporal pooling to obtain a clip embedding, followed by K sigmoid heads; optional temperature scaling is fit on the training split. Rules are mined from training labels (including depth-2 compounds) and compiled into logical DAGs; subtree gates are trained level-wise using internal-node Boolean supervision. At evaluation time, we report (i) concept prediction metrics on the validation set and (ii) consistency anomaly detection, where a clip is labeled anomalous iff it violates at least one rule under hard Boolean evaluation of the ground-truth concept vector.

B.1 Rule construction from annotations

Across datasets, our constraints are expressed as small boolean formula graphs (simple implications and depth-2 compound rules), compiled into DGL graphs and evaluated both (i) *hard* on ground-truth concept labels and (ii) *soft* on predicted concept probabilities.

Handwritten seed and compound rules (CLEVRER). For CLEVRER we include a small set of *seed* implications and a small set of *compound* depth-2 formulas (conjunctions/disjunctions under an implication). We additionally include event-structure constraints consistent with the event definitions,

e.g.

$$\text{collide}(A,B) \Rightarrow \text{collide_before_half}(A,B). \quad (24)$$

Mined pairwise implication rules. We mine high-confidence implications directly from the training concept labels by co-occurrence statistics. For each ordered pair (A, B) we estimate

$$\hat{P}(B=1 | A=1) = \frac{\#(A \wedge B)}{\#(A)}.$$

We keep candidates only if A has sufficient support, $\#(A)/N \geq \text{support_thresh}$ (default 0.05), and then add: (i) an implication $A \Rightarrow B$ if $\hat{P}(B | A) \geq \text{confidence_pos}$ (default 0.995), or (ii) an exclusion $A \Rightarrow \neg B$ if $\hat{P}(B | A) \leq \text{confidence_neg}$ (default 0.005). We cap the number of mined rules (default $\text{max_rules}=25$).

Taxonomy- and part-based rules + mined pairs (Open Images). We build implication rules from the Open Images class hierarchy and (optionally) part-of relations, restricted to the top- K selected classes. Because closure assumptions can render some “natural direction” constraints tautological (depending on how labels are completed), we also evaluate an *inverted* constraint direction that is explicitly nontrivial under label closure (e.g., coarse \Rightarrow fine, whole \Rightarrow part). Additionally, we mine high-confidence co-occurrence rules from the bounding-box validation CSV with thresholds min_support (default 200 images) and min_conf (default 0.99), and we generate a capped number of sibling-based compound rules per parent ($\text{per_parent_pair_limit}$).

Upward closure for Open Images supervision and its implications. Open Images detection annotations are not exhaustive across the taxonomy: an image may be annotated with a fine-grained class while omitting its ancestors. If missing ancestors were treated as negatives, training a multi-label concept bank would inject systematic false negatives for parent concepts (e.g., $\text{Labrador}=1$ but $\text{Dog}=0$), forcing the model to suppress parent predictions that are logically entailed by labeled descendants. To avoid this pathology, we apply an *upward hierarchical closure* to the ground-truth labels before training: whenever a class is present, all its ancestors in the provided hierarchy are marked present as well. This makes supervision consistent with the intended semantics that ancestors represent coarse presence.

A direct consequence is that *child* \rightarrow *parent* implications become tautological in the closed label space (there are no hard violations by construction), and therefore cannot define informative “consistency anomalies.” For Open Images we instead evaluate constraints that remain nontrivial under upward closure, such as *inverted* implications (coarse \rightarrow fine and whole \rightarrow part) with antecedent gating, and mined high-confidence co-occurrence implications. In this setting, flagged violations should be interpreted as *missing-detail / semantic inconsistency signals* relative to the learned concept bank and the chosen constraint family, rather than contradictions of the closed taxonomy itself.

Open-set mixture in evaluation and label-space caveats (Open Images). Although our Open Images concept inventory is restricted to a Top- K subset (for tractable multi-label learning), the *evaluation distribution* is not purely closed-set: the validation split naturally contains many instances of object subtypes outside the Top- K leaf vocabulary (e.g., unmodeled vehicle subclasses). Consequently, our reported AUROCs are measured on a realistic *mixture* of in-vocabulary and out-of-vocabulary content. This mixed setting introduces a protocol-specific label issue for implication-based constraints: when an image contains an out-of-Top- K descendant of an antecedent parent, the antecedent may be absent from the Top- K ground-truth vector used to compute rule truths (even after upward closure restricted to Top- K), rendering the implication vacuously true in the evaluation labels. This creates conservative label noise that can underestimate rule-violation detection performance.

To mitigate this, we filter evaluation samples where the image contains an out-of-vocabulary descendant of a rule antecedent (in the full Open Images label space), but that antecedent is absent in the Top- K ground-truth vector used for rule-truth computation. This situation arises because upward closure is applied only within the Top- K label space: descendants outside Top- K cannot trigger their Top- K ancestors, so the antecedent is spuriously missing and the implication is labeled vacuously true. Removing these cases reduces label-noise that would otherwise penalize methods for correctly inferring the antecedent from visual evidence.

A separate caveat concerns *hierarchical closure itself*: upward closure can activate coarse ancestors based on labeled descendants, and depending on the ontology semantics, this may not coincide with “whole object visibly present” in the scene (and may introduce its own inconsistencies). This is a generic consequence of adopting closure on a given hierarchy (shared by many closure-based pipelines) rather than a pathology specific to our Top- K implication evaluation protocol; our evaluation correction targets the former protocol-induced vacuity/coverage issue, not the closure assumption.

C Detailed Results Tables

C.1 CLEVRER – Detailed Results Tables

Table 5: CLEVRER leaf-bank evaluation on the validation split. “Prev.” denotes the number of positive validation videos for the class.

Class	Prev.	ROC-AUC	AP	Acc.@0.5
blue_sphere	2263	0.991	0.989	0.956
red_sphere	2210	0.988	0.984	0.940
green_cube	2077	0.948	0.893	0.900
yellow_cyl	2212	0.963	0.929	0.918
metal_any	4837	0.544	0.971	0.852
gray_cyl	2178	0.961	0.925	0.864
enter(shape=sphere)	2817	0.818	0.832	0.694
exit(shape=sphere)	652	0.904	0.542	0.871
enter(shape=cube)	2429	0.674	0.629	0.625
exit(shape=cube)	199	0.827	0.158	0.830
enter(shape=cylinder)	2682	0.682	0.685	0.632
exit(shape=cylinder)	310	0.835	0.257	0.808
enter(color=red)	1150	0.957	0.801	0.927
exit(color=red)	131	0.964	0.451	0.949
enter(color=green)	1122	0.954	0.782	0.915
exit(color=green)	143	0.946	0.393	0.931
enter(color=blue)	1110	0.950	0.735	0.906
exit(color=blue)	173	0.956	0.411	0.932
enter(color=yellow)	1144	0.951	0.765	0.911
exit(color=yellow)	123	0.957	0.392	0.966
enter(color=gray)	1158	0.940	0.761	0.867
exit(color=gray)	170	0.955	0.434	0.949
enter(color=brown)	1130	0.947	0.761	0.914
exit(color=brown)	157	0.952	0.384	0.940
enter(color=purple)	1126	0.961	0.783	0.913
exit(color=purple)	143	0.962	0.409	0.899
enter(color=cyan)	1184	0.952	0.777	0.906
exit(color=cyan)	171	0.951	0.460	0.938
collide(shape=sphere,shape=sphere)	1181	0.952	0.856	0.891
collide_before_half(shape=sphere,shape=sphere)	760	0.936	0.694	0.879
entered_then_collided(shape=sphere,shape=sphere)	863	0.915	0.643	0.868
collide(shape=sphere,shape=cube)	2056	0.758	0.636	0.673
collide_before_half(shape=sphere,shape=cube)	1470	0.762	0.526	0.627
entered_then_collided(shape=sphere,shape=cube)	1506	0.709	0.462	0.612
collide(shape=sphere,shape=cylinder)	2360	0.745	0.657	0.688
collide_before_half(shape=sphere,shape=cylinder)	1669	0.742	0.509	0.633
entered_then_collided(shape=sphere,shape=cylinder)	1689	0.698	0.476	0.624
collide(shape=sphere,color=red)	904	0.962	0.826	0.915
collide_before_half(shape=sphere,color=red)	589	0.947	0.653	0.902
entered_then_collided(shape=sphere,color=red)	636	0.930	0.602	0.887
collide(shape=sphere,color=green)	875	0.967	0.850	0.922
collide_before_half(shape=sphere,color=green)	566	0.954	0.689	0.907
entered_then_collided(shape=sphere,color=green)	636	0.935	0.597	0.890
collide(shape=sphere,color=blue)	929	0.962	0.838	0.914
collide_before_half(shape=sphere,color=blue)	623	0.944	0.658	0.894
entered_then_collided(shape=sphere,color=blue)	650	0.927	0.586	0.885
collide(shape=sphere,color=yellow)	912	0.968	0.857	0.914
collide_before_half(shape=sphere,color=yellow)	604	0.952	0.695	0.881
entered_then_collided(shape=sphere,color=yellow)	641	0.935	0.613	0.886
collide(shape=sphere,color=gray)	894	0.956	0.821	0.906
collide_before_half(shape=sphere,color=gray)	580	0.939	0.638	0.913
entered_then_collided(shape=sphere,color=gray)	642	0.926	0.608	0.898

Macro average: ROC-AUC = 0.900, AP = 0.659, Acc.@0.5 = 0.859

Table 6: Per-rule CLEVRER results for the **Independent-Events Probabilistic evaluator**. For readability, repeated predicate arguments within the same row are shown only on first occurrence.

ID	Rule	AUROC
01	[Chain] (collide(shape=sphere, color=brown) → collide_before_half) ∧ (collide_before_half → entered_then_collided)	0.561
02	[Chain] (collide(shape=cube, color=cyan) → collide_before_half) ∧ (collide_before_half → entered_then_collided)	0.795
03	[Chain] (collide(shape=sphere, color=green) → entered_then_collided) ∧ (entered_then_collided → collide_before_half)	0.780
04	[Chain] (collide(shape=cube, color=blue) → entered_then_collided) ∧ (entered_then_collided → collide_before_half)	0.840
05	collide(shape=sphere, shape=cube) → (collide_before_half ∧ entered_then_collided) [mined-AND; conf=0.51, hits=1041, viol=1015]	0.676
06	collide(shape=sphere, shape=cylinder) → (collide_before_half ∧ entered_then_collided) [mined-AND; conf=0.49, hits=1148, viol=1212]	0.688
07	collide(shape=cube, color=cyan) → (collide_before_half ∨ entered_then_collided) [mined-OR; conf=0.95, hits=726, viol=42]	0.679
08	collide(shape=sphere, shape=cube) → (collide_before_half ∨ entered_then_collided) [mined-OR; conf=0.94, hits=1935, viol=121]	0.515
09	collide(shape=sphere, shape=sphere) → (collide_before_half → entered_then_collided) [mined-IMP; conf=0.81, hits=961, viol=220]	0.700
10	collide(shape=sphere, color=green) → (collide_before_half → entered_then_collided) [mined-IMP; conf=0.80, hits=704, viol=171]	0.839
11	collide(shape=sphere, shape=sphere) → collide_before_half(shape=sphere, shape=sphere)	0.783
12	collide(shape=sphere, shape=sphere) → entered_then_collided(shape=sphere, shape=sphere)	0.734
13	collide(shape=sphere, shape=cube) → collide_before_half(shape=sphere, shape=cube)	0.619
14	collide(shape=sphere, shape=cube) → entered_then_collided(shape=sphere, shape=cube)	0.658
15	collide(shape=sphere, shape=cylinder) → collide_before_half(shape=sphere, shape=cylinder)	0.624
16	collide(shape=sphere, shape=cylinder) → entered_then_collided(shape=sphere, shape=cylinder)	0.651
17	collide(shape=sphere, color=red) → collide_before_half(shape=sphere, color=red)	0.855
18	collide(shape=sphere, color=red) → entered_then_collided(shape=sphere, color=red)	0.861
19	collide(shape=sphere, color=green) → collide_before_half(shape=sphere, color=green)	0.851
20	collide(shape=sphere, color=green) → entered_then_collided(shape=sphere, color=green)	0.772
21	collide(shape=sphere, color=blue) → collide_before_half(shape=sphere, color=blue)	0.830
22	collide(shape=sphere, color=blue) → entered_then_collided(shape=sphere, color=blue)	0.820
23	collide(shape=sphere, color=yellow) → collide_before_half(shape=sphere, color=yellow)	0.811
24	collide(shape=sphere, color=yellow) → entered_then_collided(shape=sphere, color=yellow)	0.789
25	collide(shape=sphere, color=gray) → collide_before_half(shape=sphere, color=gray)	0.881
26	collide(shape=sphere, color=gray) → entered_then_collided(shape=sphere, color=gray)	0.897

Table 7: Per-rule CLEVRER results for the **Neural Evaluator**. For readability, repeated predicate arguments within the same row are shown only on first occurrence.

ID	Rule	AUROC
01	[Chain] (collide(shape=sphere, color=brown) → collide_before_half) ∧ (collide_before_half → entered_then_collided)	0.895
02	[Chain] (collide(shape=cube, color=cyan) → collide_before_half) ∧ (collide_before_half → entered_then_collided)	0.891
03	[Chain] (collide(shape=sphere, color=green) → entered_then_collided) ∧ (entered_then_collided → collide_before_half)	0.883
04	[Chain] (collide(shape=cube, color=blue) → entered_then_collided) ∧ (entered_then_collided → collide_before_half)	0.893
05	collide(shape=sphere, shape=cube) → (collide_before_half ∧ entered_then_collided) [mined-AND; conf=0.51, hits=1041, viol=1015]	0.760
06	collide(shape=sphere, shape=cylinder) → (collide_before_half ∧ entered_then_collided) [mined-AND; conf=0.49, hits=1148, viol=1212]	0.728
07	collide(shape=cube, color=cyan) → (collide_before_half ∨ entered_then_collided) [mined-OR; conf=0.95, hits=726, viol=42]	0.868
08	collide(shape=sphere, shape=cube) → (collide_before_half ∨ entered_then_collided) [mined-OR; conf=0.94, hits=1935, viol=121]	0.764
09	collide(shape=sphere, shape=sphere) → (collide_before_half → entered_then_collided) [mined-IMP; conf=0.81, hits=961, viol=220]	0.856
10	collide(shape=sphere, color=green) → (collide_before_half → entered_then_collided) [mined-IMP; conf=0.80, hits=704, viol=171]	0.904
11	collide(shape=sphere, shape=sphere) → collide_before_half(shape=sphere, shape=sphere)	0.837
12	collide(shape=sphere, shape=sphere) → entered_then_collided(shape=sphere, shape=sphere)	0.881
13	collide(shape=sphere, shape=cube) → collide_before_half(shape=sphere, shape=cube)	0.602
14	collide(shape=sphere, shape=cube) → entered_then_collided(shape=sphere, shape=cube)	0.695
15	collide(shape=sphere, shape=cylinder) → collide_before_half(shape=sphere, shape=cylinder)	0.585
16	collide(shape=sphere, shape=cylinder) → entered_then_collided(shape=sphere, shape=cylinder)	0.686
17	collide(shape=sphere, color=red) → collide_before_half(shape=sphere, color=red)	0.875
18	collide(shape=sphere, color=red) → entered_then_collided(shape=sphere, color=red)	0.914
19	collide(shape=sphere, color=green) → collide_before_half(shape=sphere, color=green)	0.879
20	collide(shape=sphere, color=green) → entered_then_collided(shape=sphere, color=green)	0.915
21	collide(shape=sphere, color=blue) → collide_before_half(shape=sphere, color=blue)	0.869
22	collide(shape=sphere, color=blue) → entered_then_collided(shape=sphere, color=blue)	0.908
23	collide(shape=sphere, color=yellow) → collide_before_half(shape=sphere, color=yellow)	0.877
24	collide(shape=sphere, color=yellow) → entered_then_collided(shape=sphere, color=yellow)	0.913
25	collide(shape=sphere, color=gray) → collide_before_half(shape=sphere, color=gray)	0.875
26	collide(shape=sphere, color=gray) → entered_then_collided(shape=sphere, color=gray)	0.905

C.2 OpenImages – Detailed Results Tables

Class	Prev.	ROC-AUC	AP	Acc.@0.5	Class	Prev.	ROC-AUC	AP	Acc.@0.5
Man	3734	0.931	0.691	0.885	Tower	143	0.994	0.662	0.976
Tree	3611	0.932	0.772	0.911	Human nose	2612	0.952	0.742	0.891
Human face	3124	0.950	0.785	0.884	Bicycle wheel	245	0.993	0.806	0.942
Person	7144	0.827	0.637	0.771	Glasses	258	0.970	0.548	0.935
Woman	2775	0.942	0.720	0.889	Dress	710	0.961	0.552	0.922
Footwear	1907	0.936	0.570	0.877	Vehicle	1545	0.639	0.118	0.800
Window	904	0.937	0.414	0.868	Bird	593	0.985	0.801	0.941
Flower	2336	0.990	0.934	0.955	Street light	30	0.991	0.347	0.980
Wheel	4473	0.964	0.794	0.879	Human mouth	1979	0.950	0.641	0.868
Car	5095	0.990	0.960	0.923	Palm tree	122	0.995	0.750	0.977
Human hair	4325	0.941	0.796	0.893	Book	95	0.988	0.692	0.943
Human arm	3532	0.914	0.617	0.866	Tableware	411	0.969	0.367	0.917
Human head	3711	0.923	0.668	0.860	Drink	356	0.967	0.365	0.892
Girl	2135	0.945	0.665	0.895	Bottle	207	0.979	0.522	0.913
Building	1884	0.906	0.544	0.919	Bicycle	252	0.986	0.741	0.942
House	570	0.977	0.572	0.957	Furniture	626	0.944	0.314	0.908
Chair	311	0.973	0.607	0.926	Sculpture	190	0.972	0.319	0.924
Tire	2227	0.939	0.515	0.803	Flag	74	0.951	0.541	0.884
Suit	263	0.987	0.775	0.982	Dog	1586	0.993	0.937	0.900
Boy	579	0.938	0.328	0.910	Dessert	642	0.990	0.729	0.918
Table	593	0.962	0.455	0.927					
Skyscraper	56	0.995	0.461	0.978					
Land vehicle	1720	0.791	0.198	0.802					
Boat	567	0.992	0.806	0.949					
Jeans	285	0.955	0.343	0.916					
Human eye	1962	0.965	0.708	0.908					
Human hand	2056	0.916	0.492	0.845					
Human leg	1799	0.925	0.508	0.858					
Toy	308	0.947	0.360	0.903					

Macro average: ROC-AUC = 0.948, AP = 0.596, Acc.@0.5 = 0.904

Table 8: OpenImages leaf-bank evaluation on the validation split. “Prev.” denotes the number of positive validation images for the class.

C.3 VidOR – Detailed Results Tables

Table 11: VidOR leaf-bank evaluation on the validation split. “Prev.” denotes the number of positive validation videos for the class.

Class	Prev.	ROC-AUC	AP	Acc.@thr
Object leaves				
obj:adult	607	0.483	0.716	0.727
obj:child	299	0.625	0.442	0.640
obj:toy	115	0.688	0.219	0.862
obj:baby	122	0.697	0.245	0.854
obj:chair	65	0.641	0.119	0.922
obj:dog	73	0.622	0.122	0.913
obj:car	56	0.769	0.173	0.933
obj:table	75	0.709	0.212	0.910
obj:cup	44	0.696	0.104	0.947
obj:sofa	66	0.739	0.169	0.921
obj:ball/sports_ball	53	0.665	0.142	0.937
obj:bottle	35	0.650	0.071	0.958
obj:screen/monitor	53	0.698	0.174	0.937
obj:guitar	36	0.740	0.090	0.957
obj:cat	23	0.553	0.033	0.972
obj:backpack	30	0.657	0.068	0.964
obj:bicycle	29	0.716	0.096	0.965
obj:baby_seat	28	0.668	0.071	0.966
obj:watercraft	9	0.844	0.039	0.989
obj:bird	14	0.704	0.031	0.983
obj:laptop	15	0.758	0.075	0.982
obj:stool	13	0.733	0.051	0.984
obj:camera	22	0.490	0.034	0.974
obj:dish	8	0.806	0.078	0.990
obj:cellphone	20	0.555	0.079	0.976
obj:handbag	25	0.694	0.122	0.970
obj:duck	6	0.800	0.027	0.993
obj:horse	11	0.683	0.029	0.987
obj:motorcycle	9	0.747	0.024	0.989
obj:piano	6	0.838	0.026	0.993
obj:bench	10	0.647	0.025	0.988

Continued on next page

Class	Prev.	ROC-AUC	AP	Acc.@thr
obj:cake	6	0.754	0.016	0.993
obj:ski	12	0.755	0.031	0.986
obj:baby_walker	11	0.505	0.015	0.987
obj:elephant	4	0.845	0.019	0.995
obj:fish	4	0.634	0.008	0.995
obj:snowboard	2	0.893	0.024	0.998
obj:bat	11	0.865	0.111	0.987
obj:penguin	2	0.870	0.013	0.998
obj:chicken	2	0.559	0.004	0.998
Relation leaves				
rel:adult-in_front_of-adult	236	0.534	0.338	0.717
rel:adult-next_to-adult	239	0.578	0.351	0.714
rel:adult-watch-adult	158	0.577	0.261	0.811
rel:adult-behind-adult	151	0.530	0.190	0.819
rel:child-in_front_of-child	71	0.562	0.117	0.915
rel:child-next_to-child	65	0.603	0.126	0.922
rel:child-in_front_of-adult	127	0.610	0.196	0.848
rel:adult-watch-child	87	0.583	0.136	0.896
rel:adult-away-adult	98	0.605	0.181	0.883
rel:child-watch-child	51	0.554	0.094	0.939
rel:adult-in_front_of-child	97	0.617	0.152	0.884
rel:adult-towards-adult	73	0.528	0.101	0.913
rel:adult-next_to-child	103	0.616	0.167	0.877
rel:child-behind-child	43	0.527	0.056	0.949
rel:adult-behind-child	75	0.547	0.105	0.910
rel:child-watch-adult	55	0.664	0.116	0.934
rel:toy-next_to-toy	31	0.697	0.103	0.963
rel:child-next_to-adult	77	0.624	0.138	0.908
rel:cup-in_front_of-adult	30	0.706	0.074	0.964
rel:adult-watch-baby	45	0.696	0.104	0.946
rel:adult-next_to-table	40	0.729	0.111	0.952
rel:child-next_to-toy	56	0.699	0.125	0.933
rel:table-in_front_of-adult	32	0.703	0.071	0.962
rel:toy-in_front_of-child	45	0.676	0.101	0.946
rel:adult-next_to-cup	33	0.710	0.082	0.960
rel:baby-in_front_of-adult	59	0.694	0.124	0.929
rel:dog-next_to-dog	20	0.704	0.044	0.976
rel:child-watch-toy	34	0.668	0.063	0.959
rel:guitar-in_front_of-adult	30	0.725	0.078	0.964
rel:adult-speak_to-adult	39	0.754	0.136	0.953
rel:child-away-child	26	0.478	0.034	0.969
rel:dog-in_front_of-dog	22	0.686	0.044	0.974
rel:toy-in_front_of-adult	21	0.655	0.050	0.975
rel:child-towards-child	28	0.558	0.057	0.966
rel:bottle-in_front_of-adult	21	0.706	0.059	0.975
rel:dog-in_front_of-adult	26	0.726	0.089	0.969
rel:adult-next_to-toy	27	0.697	0.063	0.968
rel:child-away-adult	36	0.547	0.052	0.957
rel:adult-next_to-bottle	22	0.696	0.058	0.974
rel:child-towards-adult	33	0.589	0.070	0.960
rel:baby-watch-adult	21	0.665	0.046	0.975
rel:baby-next_to-toy	26	0.749	0.073	0.969
rel:dog-watch-dog	13	0.640	0.030	0.984
rel:child-hold-toy	31	0.700	0.068	0.963
rel:adult-in_front_of-baby	39	0.654	0.075	0.953
rel:child-next_to-table	30	0.786	0.168	0.964
rel:cup-next_to-cup	10	0.696	0.026	0.988
rel:adult-next_to-baby	37	0.743	0.094	0.956
rel:child-behind-adult	29	0.626	0.055	0.965
rel:adult-watch-guitar	8	0.678	0.019	0.990
rel:adult-in_front_of-screen/monitor	25	0.762	0.094	0.970
rel:adult-towards-child	19	0.664	0.041	0.977
rel:toy-in_front_of-baby	18	0.699	0.037	0.978
rel:adult-watch-dog	17	0.832	0.094	0.980
rel:toy-next_to-child	33	0.714	0.088	0.960
rel:adult-away-child	22	0.622	0.045	0.974
rel:adult-next_to-guitar	17	0.712	0.039	0.980
rel:ball/sports_ball-in_front_of-adult	16	0.702	0.067	0.981
rel:adult-in_front_of-dog	24	0.704	0.065	0.971
rel:adult-play(instrument)-guitar	28	0.735	0.071	0.966
rel:adult-behind-guitar	25	0.720	0.057	0.970
rel:table-in_front_of-child	23	0.812	0.165	0.972
rel:adult-next_to-dog	20	0.647	0.036	0.976
rel:baby-watch-toy	16	0.767	0.050	0.981
rel:adult-next_to-ball/sports_ball	17	0.622	0.046	0.980
rel:chair-in_front_of-adult	15	0.704	0.038	0.982
rel:guitar-next_to-adult	16	0.734	0.039	0.981
rel:dog-behind-dog	17	0.703	0.041	0.980
rel:adult-watch-ball/sports_ball	12	0.687	0.049	0.986
rel:bottle-next_to-bottle	5	0.735	0.016	0.994
rel:adult-next_to-backpack	16	0.700	0.062	0.981
rel:cup-next_to-adult	15	0.694	0.032	0.982
rel:table-next_to-adult	16	0.770	0.085	0.981
rel:adult-speak_to-child	24	0.716	0.068	0.971
rel:chair-next_to-chair	15	0.634	0.031	0.982

Continued on next page

Class	Prev.	ROC-AUC	AP	Acc.@thr
rel:chair-next_to-adult	18	0.674	0.036	0.978
rel:adult-lean_on-sofa	18	0.740	0.047	0.978
rel:ball/sports_ball-in_front_of-child	20	0.663	0.051	0.976
rel:adult-behind-baby	25	0.697	0.063	0.970
rel:child-next_to-ball/sports_ball	22	0.605	0.043	0.974
rel:dog-away-dog	13	0.724	0.032	0.984
rel:adult-next_to-chair	21	0.648	0.039	0.975
rel:child-in_front_of-sofa	31	0.758	0.153	0.963
rel:child-watch-ball/sports_ball	20	0.689	0.056	0.976
rel:dog-watch-adult	10	0.792	0.045	0.988
rel:chair-next_to-table	9	0.673	0.023	0.989
rel:sofa-beneath-adult	18	0.756	0.058	0.978
rel:camera-in_front_of-adult	14	0.604	0.027	0.983
rel:adult-above-sofa	18	0.759	0.058	0.978
rel:backpack-behind-adult	13	0.737	0.116	0.984
rel:toy-next_to-baby	16	0.747	0.055	0.981
rel:chair-behind-child	8	0.545	0.012	0.990
rel:cup-in_front_of-child	7	0.781	0.039	0.992
rel:adult-in_front_of-chair	13	0.713	0.056	0.984
rel:table-beneath-cup	9	0.806	0.036	0.989
rel:cup-above-table	9	0.808	0.035	0.989
rel:bottle-next_to-adult	13	0.734	0.043	0.984
rel:adult-watch-screen/monitor	8	0.725	0.025	0.990
rel:cat-next_to-cat	5	0.512	0.007	0.994
rel:adult-carry-backpack	22	0.753	0.105	0.974
rel:screen/monitor-in_front_of-adult	11	0.718	0.038	0.987
rel:adult-in_front_of-sofa	8	0.753	0.021	0.990
rel:car-in_front_of-adult	11	0.744	0.030	0.987
rel:adult-in_front_of-guitar	10	0.759	0.029	0.988
rel:cat-in_front_of-cat	3	0.465	0.004	0.996
rel:child-next_to-cup	7	0.780	0.029	0.992
rel:chair-behind-adult	13	0.733	0.047	0.984
rel:dog-next_to-adult	14	0.621	0.035	0.983
rel:child-next_to-chair	7	0.537	0.011	0.992
rel:dog-towards-dog	6	0.686	0.017	0.993
rel:chair-next_to-child	11	0.509	0.014	0.987
rel:adult-hold-cup	15	0.565	0.027	0.982
rel:sofa-behind-child	23	0.723	0.057	0.972
rel:cake-in_front_of-adult	5	0.746	0.013	0.994
rel:chair-in_front_of-child	6	0.583	0.011	0.993
rel:laptop-in_front_of-adult	9	0.743	0.027	0.989
rel:child-watch-baby	13	0.686	0.029	0.984
rel:cellphone-in_front_of-adult	12	0.543	0.019	0.986
rel:adult-watch-cake	2	0.672	0.005	0.998
rel:child-watch-cake	2	0.676	0.005	0.998
rel:child-in_front_of-screen/monitor	16	0.715	0.226	0.981
rel:adult-watch-toy	5	0.622	0.013	0.994
rel:table-in_front_of-chair	7	0.690	0.029	0.992
rel:baby-lean_on-adult	24	0.655	0.054	0.971
rel:sofa-in_front_of-adult	5	0.746	0.016	0.994
rel:adult-next_to-dish	6	0.843	0.080	0.993
rel:adult-hug-baby	20	0.639	0.042	0.976
rel:adult-ride-watercraft	6	0.831	0.027	0.993
rel:table-next_to-child	14	0.803	0.188	0.983
rel:car-behind-adult	18	0.786	0.073	0.978
rel:baby-next_to-adult	13	0.634	0.024	0.984
rel:cat-watch-cat	3	0.370	0.004	0.996
rel:adult-hit-adult	3	0.592	0.006	0.996
rel:dish-in_front_of-adult	4	0.896	0.103	0.995
rel:sofa-next_to-child	21	0.772	0.161	0.975
rel:guitar-next_to-guitar	7	0.698	0.017	0.992
rel:screen/monitor-behind-adult	15	0.730	0.050	0.982
rel:adult-hold_hand_of-adult	13	0.618	0.024	0.984
rel:child-in_front_of-chair	9	0.595	0.014	0.989
rel:adult-next_to-handbag	16	0.558	0.025	0.981
rel:car-in_front_of-car	6	0.668	0.017	0.993
rel:watercraft-beneath-adult	6	0.834	0.030	0.993
rel:child-away-chair	5	0.501	0.008	0.994
rel:car-next_to-car	5	0.758	0.014	0.994
rel:adult-above-watercraft	5	0.840	0.029	0.994
rel:adult-next_to-cellphone	14	0.570	0.022	0.983
rel:toy-next_to-adult	18	0.678	0.050	0.978
rel:baby-hold-toy	6	0.748	0.016	0.993
rel:sofa-next_to-adult	6	0.746	0.015	0.993
rel:child-next_to-bottle	6	0.626	0.015	0.993
rel:car-behind-car	8	0.678	0.020	0.990
rel:adult-hold-ball/sports_ball	6	0.704	0.060	0.993
rel:adult-behind-dog	10	0.892	0.075	0.988
rel:toy-behind-child	13	0.695	0.066	0.984
rel:adult-hold-toy	7	0.642	0.058	0.992
rel:adult-lean_on-table	14	0.754	0.047	0.983
rel:bird-next_to-bird	5	0.799	0.019	0.994
rel:dog-in_front_of-child	11	0.523	0.014	0.987
rel:sofa-in_front_of-child	15	0.711	0.166	0.982
rel:child-watch-dog	10	0.451	0.014	0.988
rel:screen/monitor-next_to-adult	13	0.678	0.046	0.984

Continued on next page

Class	Prev.	ROC-AUC	AP	Acc.@thr
rel:sofa-next_to-sofa	11	0.696	0.116	0.987
rel:adult_hold_hand_of-child	15	0.571	0.042	0.982
rel:table-behind-child	7	0.855	0.067	0.992
rel:adult-speak_to-baby	8	0.633	0.014	0.990
rel:adult-next_to-cake	6	0.777	0.017	0.993
rel:dog-away-adult	11	0.636	0.028	0.987
rel:adult-ride-bicycle	12	0.870	0.084	0.986
rel:backpack-in_front_of-adult	7	0.670	0.014	0.992
rel:dog-towards-adult	9	0.525	0.013	0.989
rel:baby-watch-child	6	0.618	0.012	0.993
rel:adult-in_front_of-laptop	9	0.712	0.021	0.989
rel:toy-in_front_of-sofa	15	0.766	0.078	0.982
rel:adult-next_to-sofa	7	0.727	0.018	0.992
rel:baby-lean_on-baby_seat	19	0.674	0.057	0.977
rel:child-towards-toy	3	0.712	0.008	0.996
rel:child-towards-chair	6	0.525	0.011	0.993
rel:handbag-next_to-adult	14	0.597	0.027	0.983
rel:piano-in_front_of-adult	5	0.835	0.025	0.994
rel:hamster/rat-next_to-hamster/rat	1	0.384	0.002	0.999
rel:table-beneath-bottle	5	0.721	0.023	0.994
rel:child-lean_on-adult	11	0.686	0.026	0.987
rel:ball/sports_ball-next_to-ball/sports_ball	8	0.621	0.014	0.990
rel:bottle-above-table	5	0.723	0.024	0.994
rel:screen/monitor-in_front_of-child	9	0.653	0.236	0.989
rel:bottle-in_front_of-child	5	0.579	0.010	0.994
rel:baby-in_front_of-child	15	0.713	0.035	0.982
rel:cake-in_front_of-child	4	0.711	0.010	0.995
rel:toy-away-toy	6	0.598	0.013	0.993
rel:child-away-toy	10	0.545	0.014	0.988
rel:child_hold_hand_of-child	1	0.560	0.003	0.999
rel:adult-away-car	15	0.759	0.049	0.982
rel:adult-caress-dog	12	0.668	0.022	0.986
rel:adult_hold_camera	13	0.573	0.021	0.984
rel:dog-next_to-toy	9	0.500	0.011	0.989
rel:sofa-next_to-table	10	0.817	0.140	0.988
rel:adult-hug-child	16	0.628	0.031	0.981
rel:adult_hold_bottle	10	0.661	0.036	0.988
rel:child-lean_on-table	10	0.832	0.069	0.988
rel:baby_seat-beneath-baby	16	0.659	0.038	0.981
rel:bicycle-beneath-adult	13	0.847	0.083	0.984
rel:ball/sports_ball-next_to-adult	6	0.507	0.010	0.993
rel:adult-above-bicycle	13	0.846	0.084	0.984
rel:adult-behind-car	13	0.710	0.055	0.984
rel:duck-next_to-duck	4	0.720	0.011	0.995
rel:child-in_front_of-dog	6	0.386	0.007	0.993
rel:bottle-next_to-cup	4	0.659	0.009	0.995
rel:adult-next_to-car	7	0.724	0.026	0.992
rel:adult-watch-cup	2	0.672	0.005	0.998
rel:cup-next_to-bottle	4	0.665	0.009	0.995
rel:adult-watch-laptop	4	0.734	0.011	0.995
rel:guitar-behind-adult	6	0.738	0.017	0.993
rel:bicycle-in_front_of-adult	9	0.553	0.014	0.989
rel:adult-behind-chair	8	0.680	0.021	0.990
rel:cat-in_front_of-adult	7	0.457	0.008	0.992
rel:toy-in_front_of-dog	7	0.403	0.008	0.992
rel:duck-in_front_of-duck	5	0.799	0.035	0.994
rel:backpack-next_to-adult	7	0.714	0.022	0.992
rel:child-lean_on-sofa	16	0.766	0.108	0.981
rel:table-behind-adult	11	0.761	0.042	0.987
rel:adult-next_to-camera	11	0.563	0.016	0.987
rel:adult-push-child	1	0.829	0.007	0.999
rel:adult-in_front_of-camera	10	0.559	0.019	0.988
rel:ball/sports_ball-next_to-toy	4	0.635	0.013	0.995
rel:child-away-sofa	5	0.683	0.013	0.994
rel:child-behind-chair	6	0.411	0.007	0.993
rel:toy-next_to-ball/sports_ball	4	0.607	0.013	0.995
rel:ball/sports_ball-away-adult	7	0.443	0.011	0.992
rel:child-next_to-baby	9	0.792	0.029	0.989
rel:adult-away-chair	6	0.769	0.031	0.993
rel:dish-next_to-dish	3	0.827	0.122	0.996
rel:child-above-sofa	14	0.777	0.121	0.983
rel:adult-lift-baby	6	0.827	0.031	0.993
rel:sofa-beneath-child	13	0.796	0.124	0.984
rel:adult-in_front_of-car	13	0.781	0.055	0.984
rel:adult-towards-car	6	0.668	0.015	0.993
rel:child_hold_ball/sports_ball	13	0.463	0.016	0.984
rel:child-watch-screen/monitor	8	0.751	0.265	0.990
rel:baby-next_to-child	11	0.659	0.021	0.987
rel:child-speak_to-child	2	0.842	0.170	0.998
rel:bird-in_front_of-bird	3	0.737	0.010	0.996
rel:adult-next_to-laptop	2	0.951	0.035	0.998
rel:screen/monitor-behind-child	10	0.665	0.157	0.988
rel:child-next_to-cake	4	0.701	0.009	0.995
rel:child-ride-bicycle	7	0.655	0.013	0.992
rel:child-next_to-dog	9	0.426	0.010	0.989
rel:baby-watch-baby	1	0.759	0.005	0.999

Continued on next page

Class	Prev.	ROC-AUC	AP	Acc.@thr
rel:adult-hold-baby	12	0.691	0.035	0.986
rel:adult-lean_on-chair	11	0.745	0.038	0.987
rel:chair-in_front_of-chair	6	0.553	0.011	0.993
rel:baby_seat-in_front_of-adult	5	0.567	0.013	0.994
rel:watercraft-next_to-watercraft	1	0.965	0.033	0.999
rel:guitar-in_front_of-child	5	0.894	0.054	0.994
rel:adult-use-camera	13	0.528	0.032	0.984
rel:baby-next_to-baby	3	0.821	0.014	0.996
rel:adult-carry-handbag	12	0.688	0.024	0.986
rel:toy-towards-toy	5	0.418	0.006	0.994
rel:cup-next_to-dish	3	0.790	0.019	0.996
rel:cat-behind-cat	0	nan	nan	1.000
rel:dish-in_front_of-child	1	0.511	0.002	0.999
rel:sofa-behind-adult	5	0.776	0.015	0.994
rel:table-next_to-chair	3	0.683	0.014	0.996
rel:cup-next_to-child	1	0.511	0.002	0.999
rel:car-next_to-adult	8	0.760	0.022	0.990
rel:baby-next_to-ball/sports_ball	7	0.653	0.016	0.992
rel:adult-next_to-stool	5	0.872	0.156	0.994
rel:laptop-next_to-adult	1	0.969	0.037	0.999
rel:toy-behind-baby	6	0.732	0.018	0.993
rel:adult-grab-ball/sports_ball	1	0.950	0.023	0.999
rel:chicken-next_to-chicken	1	0.827	0.007	0.999
rel:child-in_front_of-baby	10	0.677	0.021	0.988
rel:dish-next_to-cup	3	0.790	0.019	0.996
rel:table-in_front_of-sofa	12	0.818	0.088	0.986
rel:adult-next_to-cat	4	0.358	0.004	0.995
rel:adult-hold-cellphone	9	0.562	0.018	0.989
rel:ball/sports_ball-next_to-child	12	0.492	0.018	0.986
rel:adult-behind-camera	11	0.602	0.039	0.987
rel:child-towards-sofa	6	0.697	0.013	0.993
rel:child-next_to-sofa	14	0.733	0.108	0.983
rel:dog-watch-child	6	0.352	0.007	0.993
rel:adult-above-chair	10	0.749	0.045	0.988
rel:dish-above-table	4	0.755	0.026	0.995
rel:dog-behind-adult	5	0.851	0.032	0.994
rel:chair-beneath-adult	10	0.738	0.040	0.988
rel:bat-in_front_of-adult	8	0.865	0.103	0.990
rel:adult-away-table	6	0.627	0.011	0.993
rel:dog-bite-dog	2	0.426	0.003	0.998
rel:bottle-next_to-child	3	0.651	0.010	0.996
rel:ball/sports_ball-behind-child	8	0.631	0.016	0.990
rel:table-beneath-dish	4	0.755	0.024	0.995
rel:child-towards-ball/sports_ball	11	0.702	0.039	0.987
rel:dog-next_to-ball/sports_ball	5	0.276	0.005	0.994
rel:child-away-table	2	0.809	0.010	0.998
rel:cellphone-next_to-adult	6	0.622	0.013	0.993
rel:child-hold_hand_of-adult	8	0.545	0.056	0.990
rel:adult-watch-camera	6	0.444	0.022	0.993
rel:dog-next_to-child	8	0.336	0.008	0.990
rel:bicycle-beneath-child	9	0.661	0.027	0.989
rel:handbag-in_front_of-adult	8	0.800	0.037	0.990
rel:child-above-bicycle	9	0.663	0.024	0.989

Macro average: ROC-AUC = 0.679, AP = 0.057, Acc.@thr = 0.976

Table 12: Per-rule VidOR results for the Independent-Events Probabilistic evaluator.

ID	Rule	AUROC
001	rel:adult-watch-adult → rel:adult-next_to-adult [mined rev; sup=1111, conf=0.792, lift=2.68]	0.557
002	rel:adult-watch-adult → rel:adult-in_front_of-adult [mined rev; sup=1155, conf=0.823, lift=2.74]	0.714
003	rel:adult-away-adult → rel:adult-next_to-adult [mined rev; sup=540, conf=0.770, lift=2.60]	0.477
004	rel:adult-towards-adult → rel:adult-next_to-adult [mined rev; sup=507, conf=0.791, lift=2.67]	0.650
005	rel:adult-behind-adult → rel:adult-in_front_of-adult [mined rev; sup=1203, conf=0.914, lift=3.04]	0.451
006	rel:adult-away-adult → rel:adult-in_front_of-adult [mined rev; sup=593, conf=0.846, lift=2.81]	0.633
007	rel:adult-watch-child → rel:child-in_front_of-adult [mined rev; sup=601, conf=0.854, lift=5.51]	0.563
008	rel:child-watch-adult → rel:adult-in_front_of-child [mined rev; sup=346, conf=0.783, lift=6.89]	0.297
009	rel:adult-speak_to-adult → rel:adult-in_front_of-adult [mined rev; sup=261, conf=0.813, lift=2.71]	0.629
010	rel:child-watch-adult → rel:child-in_front_of-adult [mined rev; sup=370, conf=0.837, lift=5.40]	0.355
011	rel:adult-towards-adult → rel:adult-in_front_of-adult [mined rev; sup=581, conf=0.906, lift=3.02]	0.463
012	rel:adult-behind-child → rel:child-in_front_of-adult [mined rev; sup=597, conf=0.913, lift=5.89]	0.513

Continued on next page

ID	Rule	AUROC
013	rel:child-away-child → rel:child-next-to-child [mined rev; sup=223, conf=0.785, lift=8.40]	0.596
014	rel:child-towards-adult → rel:adult-in_front_of-child [mined rev; sup=226, conf=0.843, lift=7.43]	0.279
015	rel:child-away-child → rel:child-behind-child [mined rev; sup=214, conf=0.754, lift=11.83]	0.422
016	rel:child-towards-adult → rel:child-in_front_of-adult [mined rev; sup=222, conf=0.828, lift=5.34]	0.209
017	rel:child-behind-child → rel:child-in_front_of-child [mined rev; sup=397, conf=0.890, lift=9.53]	0.438
018	rel:adult-next-to-baby → rel:baby-in_front_of-adult [mined rev; sup=292, conf=0.872, lift=10.27]	0.296
019	rel:child-away-adult → rel:child-in_front_of-adult [mined rev; sup=247, conf=0.858, lift=5.53]	0.261
020	rel:adult-speak_to-adult → rel:adult-next_to-adult [mined rev; sup=283, conf=0.882, lift=2.98]	0.797
021	obj:baby_seat → obj:baby [mined rev; sup=203, conf=0.857, lift=5.61]	0.157
022	rel:adult-in_front_of-baby → rel:baby-in_front_of-adult [mined rev; sup=333, conf=0.915, lift=10.78]	0.467
023	rel:child-away-child → rel:child-in_front_of-child [mined rev; sup=246, conf=0.866, lift=9.27]	0.491
024	rel:adult-speak_to-adult → rel:adult-watch-adult [mined rev; sup=293, conf=0.913, lift=4.55]	0.550
025	rel:child-towards-child → rel:child-in_front_of-child [mined rev; sup=229, conf=0.895, lift=9.57]	0.635
026	obj:adult → (rel:adult-in_front_of-adult ∧ rel:adult-next_to-adult) [mined inv; ov=0.71]	0.468
027	obj:child → (rel:child-in_front_of-adult ∧ rel:adult-next_to-child) [mined inv; ov=0.72]	0.540
028	rel:adult-in_front_of-adult → (rel:adult-behind-adult ∧ rel:adult-towards-adult) [mined inv; ov=0.71]	0.464
029	obj:baby → (rel:baby-in_front_of-adult ∧ rel:adult-watch-baby) [mined inv; ov=0.94]	0.532
030	obj:toy → (rel:child-next_to-toy ∧ rel:toy-in_front_of-child) [mined inv; ov=0.91]	0.526
031	obj:dog → (rel:dog-in_front_of-adult ∧ rel:adult-in_front_of-dog) [mined inv; ov=0.84]	0.540
032	rel:baby-in_front_of-adult → (rel:adult-behind-baby ∧ rel:adult-watch-baby) [mined inv; ov=0.64]	0.597
033	obj:table → (rel:adult-next_to-table ∧ rel:table-in_front_of-adult) [mined inv; ov=0.93]	0.357
034	obj:bottle → (rel:adult-next_to-bottle ∧ rel:bottle-in_front_of-adult) [mined inv; ov=0.90]	0.593
035	obj:cup → (rel:adult-next_to-cup ∧ rel:cup-in_front_of-adult) [mined inv; ov=0.92]	0.650

Table 13: Per-rule VidOR results for the Neural Evaluator.

ID	Rule	AUROC
001	rel:adult-watch-adult → rel:adult-next_to-adult [mined rev; sup=1111, conf=0.792, lift=2.68]	0.653
002	rel:adult-watch-adult → rel:adult-in_front_of-adult [mined rev; sup=1155, conf=0.823, lift=2.74]	0.771
003	rel:adult-away-adult → rel:adult-next_to-adult [mined rev; sup=540, conf=0.770, lift=2.60]	0.677
004	rel:adult-towards-adult → rel:adult-next_to-adult [mined rev; sup=507, conf=0.791, lift=2.67]	0.626
005	rel:adult-behind-adult → rel:adult-in_front_of-adult [mined rev; sup=1203, conf=0.914, lift=3.04]	0.674
006	rel:adult-away-adult → rel:adult-in_front_of-adult [mined rev; sup=593, conf=0.846, lift=2.81]	0.696
007	rel:adult-watch-child → rel:child-in_front_of-adult [mined rev; sup=601, conf=0.854, lift=5.51]	0.778
008	rel:child-watch-adult → rel:adult-in_front_of-child [mined rev; sup=346, conf=0.783, lift=6.89]	0.505
009	rel:adult-speak_to-adult → rel:adult-in_front_of-adult [mined rev; sup=261, conf=0.813, lift=2.71]	0.897
010	rel:child-watch-adult → rel:child-in_front_of-adult [mined rev; sup=370, conf=0.837, lift=5.40]	0.657
011	rel:adult-towards-adult → rel:adult-in_front_of-adult [mined rev; sup=581, conf=0.906, lift=3.02]	0.736
012	rel:adult-behind-child → rel:child-in_front_of-adult [mined rev; sup=597, conf=0.913, lift=5.89]	0.570
013	rel:child-away-child → rel:child-next_to-child [mined rev; sup=223, conf=0.785, lift=8.40]	0.639
014	rel:child-towards-adult → rel:adult-in_front_of-child [mined rev; sup=226, conf=0.843, lift=7.43]	0.669
015	rel:child-away-child → rel:child-behind-child [mined rev; sup=214, conf=0.754, lift=11.83]	0.680
016	rel:child-towards-adult → rel:child-in_front_of-adult [mined rev; sup=222, conf=0.828, lift=5.34]	0.801
017	rel:child-behind-child → rel:child-in_front_of-child [mined rev; sup=397, conf=0.890, lift=9.53]	0.792

Continued on next page

ID	Rule	AUROC
018	rel:adult-next_to-baby → rel:baby-in_front_of-adult [mined rev; sup=292, conf=0.872, lift=10.27]	0.898
019	rel:child-away-adult → rel:child-in_front_of-adult [mined rev; sup=247, conf=0.858, lift=5.53]	0.698
020	rel:adult-speak_to-adult → rel:adult-next_to-adult [mined rev; sup=283, conf=0.882, lift=2.98]	0.659
021	obj:baby_seat → obj:baby [mined rev; sup=203, conf=0.857, lift=5.61]	0.849
022	rel:adult-in_front_of-baby → rel:baby-in_front_of-adult [mined rev; sup=333, conf=0.915, lift=10.78]	0.766
023	rel:child-away-child → rel:child-in_front_of-child [mined rev; sup=246, conf=0.866, lift=9.27]	0.785
024	rel:adult-speak_to-adult → rel:adult-watch-adult [mined rev; sup=293, conf=0.913, lift=4.55]	0.710
025	rel:child-towards-child → rel:child-in_front_of-child [mined rev; sup=229, conf=0.895, lift=9.57]	0.855
026	obj:adult → (rel:adult-in_front_of-adult ∧ rel:adult-next_to-adult) [mined inv; ov=0.71]	0.529
027	obj:child → (rel:child-in_front_of-adult ∧ rel:adult-next_to-child) [mined inv; ov=0.72]	0.731
028	rel:adult-in_front_of-adult → (rel:adult-behind-adult ∧ rel:adult-towards-adult) [mined inv; ov=0.71]	0.717
029	obj:baby → (rel:baby-in_front_of-adult ∧ rel:adult-watch-baby) [mined inv; ov=0.94]	0.841
030	obj:toy → (rel:child-next_to-toy ∧ rel:toy-in_front_of-child) [mined inv; ov=0.91]	0.829
031	obj:dog → (rel:dog-in_front_of-adult ∧ rel:adult-in_front_of-dog) [mined inv; ov=0.84]	0.737
032	rel:baby-in_front_of-adult → (rel:adult-behind-baby ∧ rel:adult-watch-baby) [mined inv; ov=0.64]	0.795
033	obj:table → (rel:adult-next_to-table ∧ rel:table-in_front_of-adult) [mined inv; ov=0.93]	0.772
034	obj:bottle → (rel:adult-next_to-bottle ∧ rel:bottle-in_front_of-adult) [mined inv; ov=0.90]	0.612
035	obj:cup → (rel:adult-next_to-cup ∧ rel:cup-in_front_of-adult) [mined inv; ov=0.92]	0.747

D Independent events formulas

Assume leaf events are **independent** *given* x , then we compute a soft satisfaction probability $P(\varphi)$ by recursion using these independent events formulas:

$$P(\neg A) = 1 - p_A, \quad (25)$$

$$P(A \wedge B) = p_A p_B, \quad (26)$$

$$P(A \vee B) = p_A + p_B - p_A p_B, \quad (27)$$

$$P(A \Rightarrow B) = 1 - P(A \wedge \neg B) = 1 - p_A(1 - p_B), \quad (28)$$

$$P(A \Leftrightarrow B) = P(A \wedge B) + P(\neg A \wedge \neg B) = p_A p_B + (1 - p_A)(1 - p_B). \quad (29)$$

E Neural Algebra of Classifiers (NAC) and similar methods, and relation to our evaluator (extended discussion).

Neural Algebra of Classifiers (NAC; Santa Cruz et al. [2018]) (other similar methods are [Misra et al., 2017, Nagarajan and Grauman, 2018, Yang et al., 2020, Li et al., 2021])) is the closest conceptual precedent to our work in that it learns neural modules intended to implement Boolean connectives and composes them along an expression tree. However, NAC composes classifier parameters (e.g., weight vectors for primitive concept classifiers) to synthesize a new classifier for a composed expression, and is trained primarily with expression-level supervision (labels for the whole composed concept). In contrast, our evaluator composes sample-level evidence through an explicit rule DAG to output clause-and rule-satisfaction probabilities, is trained with internal-node logical supervision obtained by hard propagation from ground-truth concept labels, and uses chimera operand mixing to discourage shortcut solutions and enforce operator-level compositionality locally. Finally, we introduce lineage-aware subtree caching (keyed by symbolic structure and encoder fingerprint) to reuse learned submodules safely across large rule sets and across runs, addressing scalability and representation drift in a way orthogonal to NAC’s global operator design.

The difference is that NAC can learn to evaluate, in a fully nonzero_support-supervised way, a given set of rules, and then compose to evaluate on new rules not used during training; on the other hand, in

Not-top49 class	Ancestors in Top-49
Truck	Land vehicle, Vehicle
Van	Land vehicle, Vehicle, Car
Motorcycle	Land vehicle, Vehicle
Helicopter	Vehicle
Watercraft	Vehicle
Cart	Land vehicle, Vehicle
Bus	Land vehicle, Vehicle
Train	Land vehicle, Vehicle
Tank	Land vehicle, Vehicle, Building
Wheelchair	Land vehicle, Vehicle
Taxi	Land vehicle, Vehicle
Limousine	Land vehicle, Vehicle, Car
Gondola	Boat, Vehicle
Ambulance	Land vehicle, Vehicle
Segway	Land vehicle, Vehicle
Barge	Boat, Vehicle
Golf cart	Land vehicle, Vehicle
Snowmobile	Land vehicle, Vehicle
Seat belt	Land vehicle, Vehicle

Table 9: Examples of classes outside the Top-49 whose ancestors are nevertheless present within the Top-49 set. This illustrates how hierarchical closure can introduce parent-level signals into evaluation even when the corresponding fine-grained child class is not itself included in the selected label vocabulary.

ID	Rule	Indep. Events	Neural Eval.
001	Tableware \rightarrow Bottle	0.891	0.954
002	Furniture \rightarrow Chair	0.830	0.934
003	Furniture \rightarrow Table	0.819	0.934
004	Building \rightarrow Skyscraper	0.869	0.911
005	Building \rightarrow Tower	0.867	0.908
006	Building \rightarrow House	0.843	0.887
007	Bicycle \rightarrow Bicycle wheel	0.668	0.925
008	Tree \rightarrow Palm tree	0.902	0.940
009	Vehicle \rightarrow Land vehicle	0.837	0.798
010	Land vehicle \rightarrow Bicycle	0.788	0.986
011	Land vehicle \rightarrow Car	0.722	0.829
012	Bicycle wheel \rightarrow Bicycle	nan	nan
013	Furniture \rightarrow (Chair \wedge Table)	0.854	0.938
014	Building \rightarrow (Skyscraper \wedge Tower)	0.873	0.877
015	Building \rightarrow (Tower \wedge House)	0.877	0.888
016	Land vehicle \rightarrow (Bicycle \wedge Car)	0.765	0.989

Table 10: Per-rule OpenImages results (ROC-AUC) comparing the Independent-Events probabilistic baseline and the full Neural Evaluator. Rule 012 has undefined AUROC due to degenerate evaluation labels.

our approach one can re-use only sub-rules of a bigger rule that was learned to be evaluated, but both rules didn't need any nonzero support in the training set to be learned. Thus, the strategy is to simply train our system with a very big rule containing as sub-rules all of the rules of interest, with the limiting factor only being the trade-off between the size of the total rule vs. training time, but not the nature of the training dataset itself w.r.t. to its support of the rules during supervision; nevertheless, at test time, given any sub-rule, the forward pass is simply an inference along the corresponding graph of classifiers.

One may speculate that, in NAC, the learned signal (from a fixed set of supervised training rules) will degrade at some point in a long chain of compositions, since the novel rules may be reactive to intricate correlations in uncertainty that were simply not captured by the initial set of training rules. By contrast, our local training signal at every sub-depth in the graph ensures that this should not be the case.

F Qualitative sanity-check experiment: MNIST contradiction rule

Goal. This experiment is designed as a *qualitative* diagnostic of the core ideas (rule-graphs, negation handling, learned subtree gates, and caching), not as a benchmark result. We deliberately choose a rule whose truth value is *identically false* for all inputs. The only acceptable behavior is that the learned root satisfaction probability stays near zero across the dataset, without spuriously correlating with visual styles or digit morphology.

Setup: concepts and leaf bank. We use MNIST digits as a simple controlled perceptual domain. The concept vocabulary is the 10-way one-hot digit identity:

$$y \in \{0, 1\}^{10}, \quad y_d = \mathbb{I}[\text{digit} = d], \quad d \in \{0, \dots, 9\}.$$

We train a lightweight convolutional leaf concept bank with a shared encoder and 10 sigmoid heads using multi-label BCE (even though labels are one-hot). This yields (i) encoder features $z = E_\phi(x)$ and (ii) leaf probabilities $p(x) \in (0, 1)^{10}$.

Rule graph: $A \Leftrightarrow \neg A$. Fix a target digit $n \in \{0, \dots, 9\}$ and define the atomic proposition

$$A \equiv (\text{digit} = n).$$

We compile a 3-node DGL DAG with two leaf nodes referencing the *same* concept ID (digit n) and a single root IFF node:

$$\text{root} = A \Leftrightarrow \neg A.$$

Concretely, the graph has edges (leaf \rightarrow root) with negation flags $(+1, -1)$ so that the second child is negated. Under exact Boolean semantics, this formula is false for every input:

$$\forall x, \quad (A(x) \Leftrightarrow \neg A(x)) = 0.$$

Therefore, the ground-truth root label is constant: $t_{\text{root}}(x) = 0$ for all x .

Training: single-level gate learning. Since the rule has depth 1, training reduces to learning *one* subtree gate at the root. We use the standard level-wise training procedure:

1. For each mini-batch, compute the hard truths for all nodes by bottom-up propagation from concept labels (so the root target is always 0).
2. Initialize both leaves with the encoder feature vector z (in this construction both leaves point to the same concept and thus carry the same base evidence), and pass the two child features plus negation flags into the root gate.
3. Optimize root-gate BCE loss for a small number of epochs and store the trained gate in the subtree cache keyed by the rule structure and encoder fingerprint.

A useful qualitative difference emerges when one sorts the test images of a fixed digit class by the score assigned to this contradiction rule. In this special sanity-check experiment, we use the rule output itself as the anomaly score for visualization, rather than the usual $1 - p$ transformation used for rule-satisfaction scores elsewhere in the paper. This makes the comparison especially revealing. Under the SEM variant, training sees only real normal same-image samples, which is just the full dataset in this case since no real image in it has labels that would make the truth value of this rule (which is an impossible logical assertion) nonzero. As a result, SEM receives no explicit supervisory signal that would force it to organize within-class variation according to visual abnormality; any such ordering can only arise indirectly from residual classifier uncertainty. Chimera training, by contrast, augments the same normal data with synthetic contradictory examples that are impossible in real life but are semantically ‘true’ for the rule. This provides an explicit counterfactual signal for what “abnormal” should look like at the rule level. Qualitatively, this changes the ranking behavior: although all test images shown in the figure have the same class label, the samples assigned the largest contradiction scores are visually more distorted, less prototypical, or harder to parse than those assigned the smallest scores. The chimera-trained evaluator produces a noticeably cleaner progression from normal-looking digits (left) to abnormal-looking digits (right) than SEM, suggesting that the synthetic contradictory supervision helps the model detect within-class visual abnormality rather than merely reproducing the nominal dataset label.

G Qualitative results in images

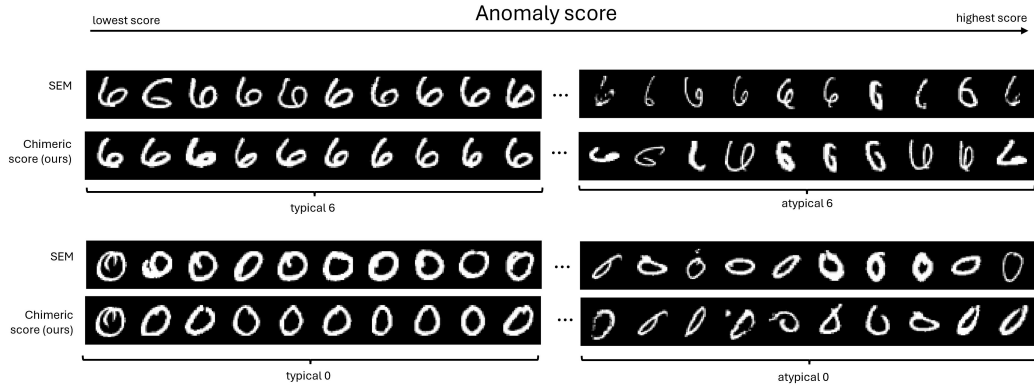


Figure 5: **Qualitative visualization of results for the MNIST contradiction rule $A \Leftrightarrow \neg A$.** In this experiment, the anomaly score is the model output for the contradiction rule itself ($\text{not } 1 - p$). SEM is trained only on real, same-image normal samples, whereas chimera training additionally introduces synthetic contradictory examples that cannot occur in real data. For a fixed test class, we sort samples by anomaly score and show the 10 smallest on the left and the 10 largest on the right. Although all shown images share the same dataset label, the high-score samples are visually more distorted and less prototypical. Chimera produces a visibly cleaner separation, tending to place more normal-looking digits on the left and more abnormal-looking ones on the right, which suggests that the synthetic contradictory supervision helps the evaluator detect within-class visual abnormality more effectively.

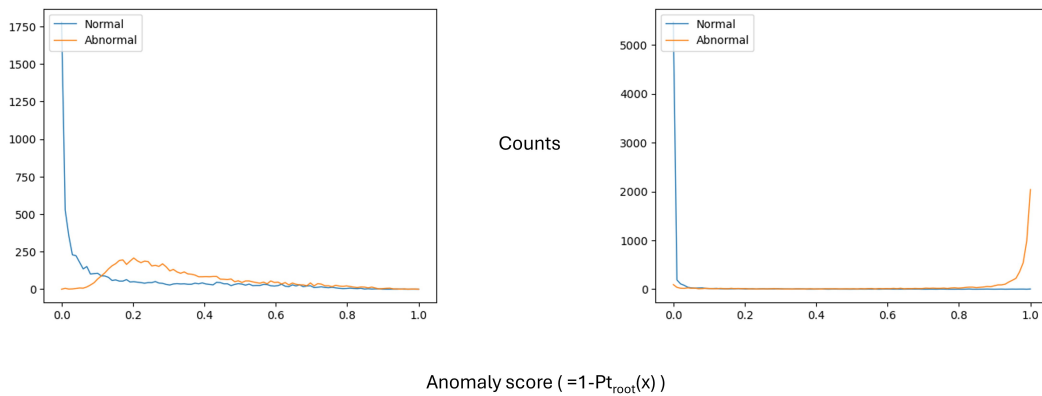


Figure 6: Anomaly score histograms corresponding to the results of the experiments in the figures below (OpenImages - Rule: Land vehicle \rightarrow (Bicycle \wedge Car)), Figs. G-8. **Left**, Indep.Events; **right**, Neural Evaluator.

OpenImages | Indep.Events | Rule: Land vehicle \implies (Bicycle \wedge Car) | AD performance:
AUROC=0.765 (green: Typical | red: Novel)



Figure 7: Showing the images from a random but *balanced* subset of the test set (i.e., same number of normal and abnormal images), with the index sorted by the anomaly score, $s_r(x) = 1 - \hat{t}_{\text{root}}^{(r)}(x)$, from low at the top left to high at the bottom right. Only displaying one every 10 images, starting from index 0. A perfect detection would show the top half of the *total* panel as normal (green framing) and the anomalies (red framing) at the bottom half.

OpenImages | Neur.Eval. | Rule: Land vehicle \Rightarrow (Bicycle \wedge Car) | AD performance:
AUROC=0.989 (green: Typical | red: Novel)



--->
Anomaly Score --->

Figure 8: Idem previous figure.

H Training protocol and architecture details

We use the implementation on the VidOR dataset as example. The implementation on the other datasets uses the same scripts with minimal adaptations to fit them.

H.1 Experimental Reproducibility Details

Codebase and implementation. All experiments use a PyTorch/DGL implementation of a feature-aware neural rule evaluator. Each logical rule is represented as a directed acyclic graph whose leaves are semantic concepts and whose internal nodes are Boolean operators. The evaluator is trained bottom-up from leaves to root: each internal gate maps child features, together with edge-level negation flags, to a parent feature and a parent truth probability. The implementation uses DGL graph traversal for the rule structure, PyTorch modules for the leaf bank and subtree gates, and scikit-learn for AUROC/AP evaluation.

Rule evaluator and caching. For each rule graph, internal modules are trained level-wise by node depth. The implementation uses lineage-aware subtree caching: cache keys include the exact symbolic subtree, edge order/negations, gate architecture tag, feature dimensionality, and a fingerprint of the upstream encoder. This prevents accidental reuse of subtree gates when the feature-producing encoder changes. At inference, the trained or cached gates are applied level-by-level until the root truth probability is obtained.

H.2 Dataset Construction and Splits

VidOR data layout. The VidOR experiments assume the following directory layout:

```
<vidor_root>/annotations/{train,val}/*.json,  
    <vidor_root>/videos/<video_path>.
```

If the annotation does not directly provide a resolvable video path, the code falls back to a video identifier lookup. The train split is used for concept mining, rule mining, leaf-bank training, rule-gate training, optional calibration, and optional learned aggregation. The validation split is used for final anomaly scoring and reported AUROC.

Semantic leaf vocabulary. The VidOR leaf vocabulary consists of object atoms and relation atoms:

```
obj : <category>,    rel : <subject>-<predicate>-<object>.
```

The object vocabulary is selected from the most frequent training categories, and the relation vocabulary is selected from the most frequent training subject–predicate–object triples after applying the minimum relation-support threshold. In the reported configuration, the default budgets are

$$K_{\text{obj}} = 40, \quad K_{\text{rel}} = 200, \quad \text{min_rel_support} = 20,$$

unless otherwise stated in the experiment table.

Video preprocessing. Each video is represented by uniformly sampled frames. The default VidOR configuration uses

$$T = 8 \text{ frames per clip}, \quad 224 \times 224 \text{ spatial resolution}.$$

At training time, optional augmentation consists of resizing, color jitter, random affine perturbations, tensor conversion, and random erasing. At validation time, only resizing and tensor conversion are applied.

H.3 Model Architecture

Leaf bank. The VidOR leaf bank is a multi-label video classifier. For each clip, a frame-level CNN backbone is applied to the sampled frames, the resulting frame embeddings are projected to a feature dimension F , and the projected frame embeddings are mean-pooled across time. The pooled feature is fed into K independent linear heads, one per semantic leaf. The default backbone is ImageNet-pretrained ResNet-18, with a lightweight convolutional alternative available. The default feature dimension is

$$F = 256.$$

Subtree gate. Each internal node of arity a uses a local gate

$$g_\theta : \mathbb{R}^{a(F+1)} \rightarrow \mathbb{R}^F \times (0, 1),$$

where the input concatenates each child feature with a scalar edge-negation flag. The gate is an MLP with ReLU nonlinearities followed by a sigmoid truth head:

$$(h_v, \hat{p}_v) = g_{\theta_v}([h_{c_1}, b_1, \dots, h_{c_a}, b_a]).$$

The output h_v is used as the parent feature for higher nodes, and \hat{p}_v is the predicted truth probability for the subformula rooted at v .

H.4 Training Protocol and Hyperparameters

Optimization. The leaf bank is trained with binary cross-entropy with logits. When class-count statistics are enabled, positive-class weights are computed from training-set prevalence. The default optimizer for the leaf bank is Adam with learning rate

$$\eta_{\text{leaf}} = 10^{-3},$$

weight decay 0 unless otherwise stated, and default training duration of 3 epochs.

Level-wise evaluator training. For every rule graph, subtree gates are trained bottom-up by depth. At each level, hard truth targets for all graph nodes are computed from ground-truth leaf labels using exact Boolean propagation. The gate at each internal node is optimized with binary cross-entropy against its node-level Boolean truth target. The default evaluator training hyperparameters are:

$$\eta_{\text{level}} = 10^{-3}, \quad \text{epochs_level} = 2, \quad \text{batch_train} = 64.$$

Chimera-only operand training. All reported runs use (except in the ablations that use only the normal class during training)

`-negatives chimeras_only.`

In this mode, the operands of each binary gate are constructed from different samples in the mini-batch. For a batch permutation π with $\pi(i) \neq i$, the left operand is taken from sample i and the right operand from sample $\pi(i)$. The target is computed by applying the Boolean operator to the corresponding hard child truth values:

$$t_i^{\text{chim}} = \text{op}(t_\ell(y_i), t_r(y_{\pi(i)})).$$

Both positive and negative chimera cases are used, depending on whether the operator evaluates to true or false.

Temperature calibration. When enabled, post-hoc temperature scaling is fit on the training split using binary cross-entropy on the leaf logits. The learned scalar temperature is saved and reloaded at evaluation time.

Default run configuration. Unless explicitly overridden in the experiment table, the VidOR runs use:

Backbone	ResNet-18
Feature dimension	256
Frames per clip	8
Resize	224 × 224
Leaf epochs	3
Rule-gate epochs per level	2
Leaf learning rate	10 ⁻³
Rule-gate learning rate	10 ⁻³
Batch size, train/eval	64/64
Rule aggregation	min
Implication gate threshold	0.0
Random seed	123.

H.5 Evaluation Protocol

Leaf-level evaluation. For the leaf bank, we report per-class ROC-AUC, average precision, and accuracy at threshold 0.5 on the validation split. Macro summaries are computed over valid classes, ignoring degenerate classes for which ROC-AUC or AP is undefined.

Rule-level scores. For each rule r , the evaluator produces a predicted rule-satisfaction probability

$$\hat{p}_r(x) \in (0, 1).$$

The per-rule violation score is

$$v_r(x) = 1 - \hat{p}_r(x).$$

AUROC computation. The main anomaly metric is AUROC against the pseudo-anomaly label

$$Y_{\text{anom}}(x) = 1 - \min_r T_r(y),$$

where $T_r(y) \in \{0, 1\}$ is the exact Boolean truth value of rule r under ground-truth leaves. Per-rule AUROC is also computed by comparing $1 - \hat{p}_r(x)$ against $1 - T_r(y)$. If the validation labels are all normal or all anomalous under the pseudo-ground-truth, AUROC is reported as undefined rather than forced to a numeric value.

H.6 Compute and Software Environment

Software dependencies. The experiments require Python with PyTorch, torchvision, DGL, OpenCV, Pillow, scikit-learn, NumPy, and tqdm. The code selects CUDA automatically when available and otherwise falls back to CPU.

Hardware. The experiments were run on a NVIDIA H100 GPU.

Runtime controls. The most important runtime controls are the number of sampled frames, image resize, batch size, number of workers, number of leaf epochs, number of evaluator epochs per level, and the number of retained rules. The code supports `-train_frac` for controlled training-set subsampling and `-train_missing_only` for reusing existing cached gates when applicable.

H.7 Randomness and Determinism

The code sets the Python random seed and the PyTorch CPU seed, and also sets the CUDA seed when CUDA is available. The default seed is

123

for the VidOR experiments. Remaining nondeterminism can arise from GPU kernels, data-loader worker scheduling, video decoding, and randomized data augmentation.

H.8 Data, Licenses, and Ethics

Dataset access. We use existing third-party datasets and do not introduce a new dataset. The VidOR files are expected to be obtained from the official dataset distribution and arranged in the directory structure described above.

Annotations and labels. The anomaly labels used in our experiments are pseudo-labels derived from logical inconsistency under retained semantic rules, not human judgments of abnormality. Therefore, the reported anomaly-detection results should be interpreted as rule-consistency detection under a selected concept vocabulary and selected rule set.

Privacy and human subjects. The experiments use pre-existing public video annotations and do not involve newly collected human-subject data. No attempt is made to identify individuals. If any dataset split contains people, the analysis is restricted to the dataset-provided object and relation categories.

Limitations and potential misuse. The method can flag violations of explicit rules, but it inherits errors from the leaf bank, biases from dataset annotations, and biases from mined rule selection. A high anomaly score should therefore be interpreted as evidence of semantic inconsistency relative to the selected rule set, not as a general-purpose safety or surveillance judgment. The system should not be deployed for consequential decisions without validating the rule set, concept vocabulary, calibration, and false-positive/false-negative behavior in the target domain.